AN INVESTIGATION INTO THE WEAR BEHAVIOR AND DEBRIS PARTICLE FORMATION OF ULTRA HIGH MOLECULAR WEIGHT POLYETHYLENE

A Dissertation

by

KEVIN GRANT PLUMLEE

Submitted to the Office of Graduate and Professional Studies of
Texas A&M University
in partial fulfillment of the requirements for the degree of

DOCTOR OF PHILOSOPHY

Chair of Committee,	Harry Hogan
Committee Members,	Melissa Grunlan
	Hong Liang
	Hung-Jue Sue
Head of Department,	Andreas Polycarpou

May 2018

Major Subject: Mechanical Engineering

ABSTRACT

Ultra-high molecular weight polyethylene (UHMWPE) is a popular choice for bearing material due to its low wear and low friction coefficient. It remains the primary material for use in artificial joints, which has led to an extensive history of tribologic study, and has resulted in a variety of techniques for reducing total wear volume. However, very little is known regarding the actual mechanisms that lead to individual debris particle formation. Applying well-established wear testing techniques specifically to explore UHWMPE wear mechanisms may open new insights and new possibilities for engineering long lasting joints.

First, wear debris image analysis was applied to debris collected after UHMWPE pins were worn against counterfaces of three different roughnesses, and then imaged in a scanning electron microscope. The debris was characterized using standard analysis techniques: equivalent circle diameter (ECD), roundness factor, and Richardson fractal dimension. Results revealed evidence of abrasion, adhesion and fatigue processes, but a large percentage of particles were small and smooth, and were not easily classified. It is hypothesized that these particles are the result of plastic deformation at the wear interface.

Analysis of the resultant wear surface of UHMWPE samples is also suggestive of plastic deformation, including an often observed but never explained *ripple* pattern. Computer modeling supports the notion that deformation takes place at the surface, which led to the conclusion that a thin layer of strained polymer can buckle during relaxation, resulting in a rippled geometry. In this case, the final ripple wavelength would be determined by the thickness of the deformed layer.

To test this hypothesis, computer models were used to predict the effects of contact pressure, temperature, and counterface roughness on the rippled surface geometry. Corresponding experimental tests did reveal high levels of plastic deformation, but in much thinner sections than anticipated. Additionally, the experimental effects of pressure and temperature did not match the simulations and suggested that the ripple formations are more dynamic than previously thought, and are the result of a thin, self-adhering transfer film rather than straining of the bulk polymer itself.

ACKNOWLEDGEMENTS

I would like to thank my committee chairs, Dr. Schwartz and Dr. Hogan, and my committee members, Dr. Sue, Dr. Liang, and Dr. Grunlan, for their guidance and patience throughout the course of this research. Special thanks to Dr. Bishop, who agreed to sit in on my defense and provide value expertise in from the biomedical perspective. I would also like to thank my current employer, Oklahoma Christian University, for their support, patience, and accountability while I finished this dissertation.

Special thanks also go to my friends and colleagues at the Microscopy and Imaging Center at Texas A&M University, and the Sam Noble Microscopy Laboratory at the University of Oklahoma. They have gone above and beyond in accommodating my needs, and have been friendly and informative throughout my work.

Finally, thanks to my mother and father for their encouragement, to my sister for the laughs, and especially to my wife for her patience and love.

CONTRIBUTORS AND FUNDING SOURCES

This work was supervised by a dissertation committee consisting of Dr. C. Schwartz, advisor and committee chair (currently serving as Director of Undergraduate Research at Iowa State University), and Dr. H. Hogan, who served as the Texas A&M University co-chair of the committee. Other committee members include Dr. H.J. Sue and Dr. H. Liang of the Department of Mechanical Engineering and Dr. M. Grunlan of the Department of Biomedical Engineering.

The work presented in Chapter I and II was completed by the author, and was funded by a fellowship from Texas A&M University. The work presented in Chapter III was funded by Oklahoma Christian University. Custom experimental equipment discussed in Chapter III was designed and assembled by undergraduate students at Oklahoma Christian University under the direction of the author, but all experiments and analysis presented in this dissertation was performed by the author.

TABLE OF CONTENTS

Page

LIST OF FIGURES

Page

LIST OF TABLES

Page

1. INTRODUCTION AND LITERATURE REVIEW

Wear and friction are a part of virtually every mechanical system, and as such, they serve as a major contributor of difficulties and complications, ranging from detriments in efficiency and power to the time and financial cost of component maintenance and replacement. In a study in 1990, Jost reported that between 1 and 2% of the GNP could be saved by appropriate application of tribology research and education [1]. Polymers have been particularly successful in addressing these tribologic issues due to their low wear, low friction, and ease of manufacture. Polymers are often self-lubricating, requiring little maintenance; they are lightweight and resistant to most chemicals, but often wear down quickly compared to the metal counterparts.

One particularly noteworthy polymer in tribology is ultra-high molecular weight polyethylene (UHMWPE), which is used in many applications, extending from bearings and bushings to cutting boards to artificial joints. For example, UHMWPE is currently the predominant bearing material used in artificial joints, with approximately one million operations performed each year and seven million Americans living with replaced hips or knees [2, 3]. Despite its naturally low wear rate, low coefficient of friction, and natural biocompatibility in its bulk from, UHMWPE has a major downfall: the microscopic wear debris that is generated within the body results in an immune system response, which ultimately leads to a condition known as osteolysis, where the bone surrounding the implant degenerates [4, 5].

In a similar vein, environmental advocates have also taken notice of the negative effects of polymer wear debris, finding that dust on the road is the third largest contributor of airborne particles in urban settings [6]. This dust is comprised partly of debris from worn tires and brake linings [7], is readily inhaled [8, 9], and has chemical composition that can cause major health risks [10-12]. Understanding the mechanisms that lead to the formation of polymer wear debris could lead to improved wear performance and reap a reward of health benefits for the public.

Naturally, the magnitude of the consequences of wear debris has generated a significant amount of research over the last 25 years, primarily focused on reducing polymer wear rates in general. These efforts aim to extend product life and reduce the negative effects of the resulting debris particles. One technique that has proven successful in the case of UHMWPE is crosslinking the polymer through chemical processing [13, 14] or irradiation [15]. Crosslinking drastically reduces the total wear volume of UHMWPE under the assumption that less total volume of debris will lead to less osteolytic response of artificial joints [15-19]. Unfortunately, recent studies show that the immune system response is not only affected by the total wear rate, but also by the size and shape of the debris [20, 21] and that crosslinking may not be effective in reducing the number of particles generated within the most bio-active size range (≤ 1.0 μm) [22-24].

Another common approach to improving any polymer performance is the introduction of composite fillers. But the general lack of depth in understanding of polymer wear mechanisms means that many of the attempts to use composites in tribology have been implemented in a guess-and-check fashion with little-to-no basis for their

reasoning. Expectedly, not all of these techniques successfully reduce the wear rate [25, 26], and even those that do may not reduce potential negative health effects [23, 27, 28]. In the case of UHMWPE, a substantial number of studies have focused on using composite fillers to reduce total wear volume [29-31]. The range of fillers used is representative of the variety of potential wear mechanisms involved. Large, hard particles have been incorporated to strengthen the matrix and act as a load shield [25, 26, 32-36], including the use of specifically biocompatible materials [37-40]. Other fillers include the addition of soft materials for compliance and impact resistance, nano-composites (both fibers and clays) [41-46], and fluoropolymers for reduced friction coefficient [47, 48]. The use of additional materials into the wear surface results in more complicated wear dynamics and more complicated health factors.

Despite the success of polymer bearings in general, and the extensive research into wear reduction techniques, very little is known about debris formation mechanisms. Most of the vocabulary used to describe polymer wear has been inherited from the longer tradition of metal tribology, including mechanisms like *abrasion, adhesion, fatigue, and corrosion* [49]. Unfortunately, these terms have loose definitions and significant overlap with each other. *Abrasion* typically refers to when material is removed through the mechanical interlocking of the soft material by a single pass of a hard asperity [50, 51] and typically requires sufficiently rough counterfaces. *Adhesive wear* can refer to any case in which the molecular attraction forces between the polymer and the counterface contribute a significant portion of the stress state of the polymer, which often occurs with smooth counterfaces [52]. However, within polymer wear, the term *adhesion* often

specifically refers to a situation in which the debris adheres to the counterface after removal from the bulk [52-54]. *Fatigue wear* is typically characterized by cyclic stress states that promote crack propagation through a material [55]. *Corrosion effects* are typically less of a concern with polymers, although the thermal effects of friction can influence properties and performance greatly [52, 56]. It is unlikely that any one of these mechanisms is singly responsible for a specific polymer's wear behavior.

Direct observation of individual particle formation is inherently difficult, due in part to the size scale and restricted access of the mating surfaces. In an effort to distinguish and describe the various mechanisms for polymer wear, a variety of experimental techniques are employed to compare observe polymer behavior. The majority of these techniques are dependent on the analysis of the end-products after the wear process, such as the resultant wear debris [57-63] and wear surface geometry [15, 64, 65]. One polymer that has been extensively studied in wear and friction is polytetrafluoroethylene (PTFE), most notable for its extremely low coefficient of friction. PTFE gains much of its reputation thanks to its low shear strength, which allows the deposition of a thin layer of polymer onto the counterface, which effectively acts as a lubricant [66]. This transfer layer is easily visible under microscopic viewing of the counterface and is a clear indicator of adhesion and resultant shearing of the polymer bulk. Additionally, the debris that results from such wear mechanisms tend to be reasonably large, flat flakes. The introduction of fillers complicates issues and can improve the resilience of the transfer film [67], or can retard and hinder the development of the film and reduce ductility and abrasion resistance of the polymer bulk [68, 69].

UHMWPE is also a popular friction material and is similar in molecular structure to PTFE, although its wear mechanisms and volumetric wear rates are different. UHWMPE does not classically show signs of fatigue cracking and is moderately abrasion resistant [70]. UHMWPE does generate a weak transfer film in certain circumstances, but rarely creates a fully coherent or continuous film [71, 72]. Additionally, UHMWPE wears significantly slower than PTFE, with up to 50 times less wear volume [73]. Despite many years of vigorous study, many different mechanisms have been ascribed to polyethylene, including abrasion [74], adhesion [40, 75], fatigue [16, 76], and accumulation of plastic deformation [32, 77].

Of particular interest is a surface phenomena in which the smooth, worn surface of UHWMPE develops a periodic and regular rippled topography. In 1978, Charnley and Dowling, pioneers of the artificial hip, described the phenomenon: "The cause of the parallel ripples has not yet been identified," and commented that why the multi-direction wear behavior "should produce such an oriented topography is hard to explain" [78]. Over 20 years later, Wang *et al* commented on the same phenomena: "It is still not well understood how the ripples are formed... but it is generally accepted that accumulated plastic deformation plays a critical role in the formation of the ripple-like features on the surface of the acetabular cups" [77]. Possible explanations for this feature range from abrasion [74], crystal lamellae alignment [79], chain alignment [32, 80], fatigue [76, 81], thermal softening due to friction [82, 83], flow instability (shark skinning) [84], Shallamach waves [85], and stick-slip [86, 87]. There is currently no consensus among

researchers and little is known about their formation or which factors dominate their creation.

The technique of fitting various properties to experimental results via mathematical models has frequently been employed in an effort to gain insight into which parameters and properties are most significant. Many times, these math models are based on physical behaviors and well understood principles, as in the case of the well-known Archard model, which states that the total wear volume is linearly proportional to work done by friction [88]. While this model fits well in many metals, it does not accurately predict the wear of most plastics. The Ratner-Lancaster model typically applies plastics [50, 89], although it does not fit UHMWPE particularly well [90]. Further models have added additional test parameters and material properties to the best-fit curves. Jain and Bahadur developed a model based on fatigue with similar results to the these models [91], while Kraghelsky's model for elastic polymers resulted in a more complicated model [92]. The model by Chowdhury and Chakraborti includes generalized descriptions for two main mechanisms, abrasion and fatigue, and includes dozens of material properties and parameters [93]. Viswanath and Bellow attempted to apply Buckingham Pi theory to their model, resulting in five different non-dimensional terms that each represent a different facet of the wear process, from material properties to test parameters, and then applied to a non-linear model [94]. Meng and Ludema reviewed over 300 equations for wear. While many of these models match the data with good approximation (which is to be expected for a best-fit curve), they sum up their results with "no single predictive equation or group of limited equations could be found for general and practical use" [95].

For such complicated systems, it is natural to turn to the use of computer simulations to help visualize the physical processes. Finite element models, using continuum mechanics equations, are the most common simulations, although most are focused on bulk loading profiles of larger components, and not wear mechanisms or wear rates [96-99]. To isolate specific wear mechanisms, some researchers have used finite element models to explore the deformation and possible removal of material at a singular asperity [81, 100]. These models reveal that plastic deformation occurs at the surface of the polymer, while Mirghany used finite element models to demonstrate that, in the case of third body wear, stresses are high enough to plastically deform both the polymer and counterface [101]. Unfortunately, the high levels of deformation, material property changes, and ultimate material failure results in finite element models being extremely inaccurate when used to model removal of material. Additionally, the size scale of debris and surface interactions may negate the continuum mechanics assumptions of finite modeling altogether [102]. To overcome the scaling issues, molecular dynamics models can simulate the molecular motion of individual polyethyelene chains, including amorphous and crystalline regions. These models are limited to a small number of atoms and simplified loads and interactions, such as crystallization processes [103-105] or uniaxial tension [106-108]. Modern technological advances have increased the number of atoms that can be included in the simulation and now have been successfully implemented to simulate nano-filler interactions [109-111] and lubrication dynamics [112]. However, currently, most simulated test geometries are still in the range of tens of nanometers across

and include tens of thousands of atoms; this is a far cry from the micron-size level of asperity contacts and the hundreds of thousands of atoms in a single chain of UHWMPE.

Regardless of the simulation method used, accurate material properties are required to achieve accurate results. Unfortunately, semi-crystalline polymers, such as polyethylene, are both multi-phase and viscoelastic, making modeling particularly challenging in this regard. Their properties vary greatly due to level of crystallinity, chain alignment (particularly during plastic deformation), temperature, and loading rates. In the case of tribology, all of these parameters vary over time, as friction and plastic deformation change the local temperature and level of strain of the polymer. Thusly, UHMWPE has been studied for a variety of conditions and properties [16, 55, 113, 114]. For example, during plastic deformation, the quantity and morphology of crystalline regions also change [114-116]. Other curiosities also emerge; for example, while crosslinking has been shown to reduce volumetric wear rate drastically, it only marginally changes the most commonly described mechanical properties [117]. Despite reductions in elongation due to crosslinking, plastic deformation has been shown to play a critical role in wear in both crosslinked and virgin cases [77, 118, 119]. Without clear direction into what properties, parameters, and mechanisms are in effect, it is unlikely that simulations will accurately model the complex micro- and macro- behavior of polymers during wear processes. A simulation is only as good as the information input into it.

Until the understanding of molecular behavior of UHWMPE grows substantially, along with a corresponding increase in computational power, the best techniques for understanding wear debris formation in UHMWPE still rely on experimentation and

subsequent observation of resultant wear surfaces and debris. Unfortunately, the majority of efforts have focused on reducing volumetric wear rates, not understanding mechanisms. There are studies that have collected and analyzed wear debris for its biological effect [20, 21, 24], but little focus has been on using those results to discern wear mechanisms. Similarly, viewing the resultant wear surface of the remaining bulk polymer is a common practice and researchers have observed the formation of a periodic, directional, rippled surface geometry for many decades. Nevertheless, there is no consensus on the process that creates this surface geometry or which factors influence the formation of wear debris.

Even still, the many years of study of UHMWPE have led to a greater understanding of its wear behavior. Well-established techniques for generating specimens and collecting debris already exist, and most computer simulations and researchers agree that plastic deformation plays a critical role in wear in general. This study aims to apply these techniques with a renewed emphasis on understanding the mechanisms and parameters that cause wear debris, not only to deepen the knowledge of polymer tribology in general, but also to open new approaches for reducing the negative health effects of wear debris.

1.1 References

[1] H.P. Jost, Tribology — Origin and future, Wear, 136 (1990) 1-17.

[2] A.J.R. Registry, Annual Report 2016, 2016.

[3] H. Maradit Kremers, D.R. Larson, C.S. Crowson, W.K. Kremers, R.E. Washington, C.A. Steiner, W.A. Jiranek, D.J. Berry, Prevalence of Total Hip and Knee Replacement in the United States, The Journal of Bone and Joint Surgery. American volume, 97 (2015) 1386-1397.

[4] J.H. Dumbleton, M.T. Manley, A.A. Edidin, A literature review of the association between wear rate and osteolysis in total hip arthroplasty, The Journal of Arthroplasty, 17 (2002) 649-661.

[5] N.D.L. Burger, P.L. de Vaal, J.P. Meyer, Failure analysis on retrieved ultra high molecular weight polyethylene (UHMWPE) acetabular cups, Engineering Failure Analysis, 14 (2007) 1329-1345.

[6] L.M. Hildemann, G.R. Markowski, G.R. Cass, Chemical composition of emissions from urban sources of fine organic aerosol, Environmental Science & Technology, 25 (1991) 744-759.

[7] W.F. Rogge, L.M. Hildemann, M.A. Mazurek, G.R. Cass, B.R.T. Simoneit, Sources of fine organic aerosol. 3. Road dust, tire debris, and organometallic brake lining dust: roads as sources and sinks, Environmental Science & Technology, 27 (1993) 1892-1904.

[8] B.D. Garg, S.H. Cadle, P.A. Mulawa, P.J. Groblicki, C. Laroo, G.A. Parr, Brake Wear Particulate Matter Emissions, Environmental Science & Technology, 34 (2000) 4463-4469.

[9] A. Iijima, K. Sato, K. Yano, H. Tago, M. Kato, H. Kimura, N. Furuta, Particle size and composition distribution analysis of automotive brake abrasion dusts for the evaluation of antimony sources of airborne particulate matter, Atmospheric Environment, 41 (2007) 4908-4919.

[10] O. von Uexküll, S. Skerfving, R. Doyle, M. Braungart, Antimony in brake pads-a carcinogenic component?, Journal of Cleaner Production, 13 (2005) 19-31.

[11] M.S. Happo, M.-R. Hirvonen, A.I. Hälinen, P.I. Jalava, A.S. Pennanen, M. Sillanpää, R. Hillamo, R.O. Salonen, Chemical Compositions Responsible for Inflammation and Tissue Damage in the Mouse Lung by Coarse and Fine Particulate Samples from Contrasting Air Pollution in Europe, Inhalation Toxicology, 20 (2008) 1215-1231.

[12] D.B. Warheit, C.M. Sayes, K.L. Reed, K.A. Swain, Health effects related to nanoparticle exposures: Environmental, health and safety considerations for assessing hazards and risks, Pharmacology & Therapeutics, 120 (2008) 35-42.

[13] J.d. Boer, A.J. Pennings, Crosslinking of ultra-high molecular weight polyethylene in the melt by means of 2,5-dimethyl-2,5-bis(tert-butyldioxy)-3-hexyne: 2. Crystallization behaviour and mechanical properties, Polymer, 23 (1982) 1944-1952.

[14] J.R. Atkinson, R.Z. Cicek, Silane cross-linked polyethylene for prosthetic applications Part I. Certain physical and mechanical properties related to the nature of the material, Biomaterials, 4 (1983) 267-275.

[15] O.K. Muratoglu, C.R. Bragdon, D.O. O'Connor, M. Jasty, W.H. Harris, A novel method of cross-linking ultra-high-molecular-weight polyethylene to improve wear, reduce oxidation, and retain mechanical properties: Recipient of the 1999 HAP Paul Award, The Journal of Arthroplasty, 16 (2001) 149-160.

[16] E. Oral, S.D. Christensen, A.S. Malhi, K.K. Wannomae, O.K. Muratoglu, Wear Resistance and Mechanical Properties of Highly Cross-linked, Ultrahigh-Molecular Weight Polyethylene Doped With Vitamin E, The Journal of Arthroplasty, 21 (2006) 580-591.

[17] G. Lewis, Properties of crosslinked ultra high molecular weight polyethylene, Biomaterials, 22 (2001) 371-401.

[18] M. Jasty, H.E. Rubash, O. Muratoglu, Highly cross-linked polyethylene: the debate is over--in the affirmative, J Arthroplasty, 20 (2005) 55-58.

[19] R. Chiesa, M.C. Tanzi, Alfonsi, Paracchini, Moscatelli, Cigada, Enhanced wear performance of highly crosslinked UHMWPE for artificial joints, Journal of Biomedical Res., 50 (2000) 381-387.

[20] T.R. Green, J. Fisher, J.B. Matthews, M.H. Stone, E. Ingham, Effect of size and dose on bone resorption activity of macrophages by in vitro clinically relevant ultra high molecular weight polyethylene particles, Journal of Biomedical Materials Research, 53 (2000) 490-497.

[21] J.A. Savio, L.M. Overcamp, J. Black, Size and shape of biomaterial wear debris, Clinical Materials, 15 (1994) 101-147.

[22] J.H. Ingram, M. Stone, J. Fisher, E. Ingham, The influence of molecular weight, crosslinking and counterface roughness on TNF-alpha production by macrophages in response to ultra high molecular weight polyethylene particles, Biomaterials, 25 (2004) 3511-3522.

[23] M.D. Ries, Highly cross-linked polyethylene: the debate is over--in opposition, J Arthroplasty, 20 (2005) 59-62.

[24] A. Galvin, J. Tipper, Nanometre size wear debris generated from crosslinked and non-crosslinked ultra high molecular weight polyethylene in artificial joints, Wear, 259 (2005) 977-983.

[25] J. Tong, Y. Ma, M. Jiang, Effects of the wollastonite fiber modification on the sliding wear behavior of the UHMWPE composites, Wear, 255 (2003) 734-741.

[26] B.-P. Chang, H. Md. Akil, R. Bt. Md. Nasir, Comparative study of micro- and nano-ZnO reinforced UHMWPE composites under dry sliding wear, Wear, 297 (2013) 1120-1127.

[27] J. Fisher, J. Bell, P. Barbour, J. Tipper, J. Mattews, A. Besong, M. Stone, E. Ingham, A novel method for the prediction of functional biological activity of polyethylene wear debris, Proceedings of the Institution of Mechanical Engineers, Part H: Journal of Engineering in Medicine, 215 (2001) 127-132.

[28] J.A. Puértolas, S.M. Kurtz, Evaluation of carbon nanotubes and graphene as reinforcements for UHMWPE-based composites in arthroplastic applications: A review, Journal of the Mechanical Behavior of Biomedical Materials, 39 (2014) 129-145.

[29] S. Ramakrishna, J. Mayer, E. Wintermantel, K.W. Leong, Biomedical applications of polymer-composite materials: a review, Composites science and technology, 61 (2001) 1189-1224.

[30] J. Bijwe, Composites as friction materials: Recent developments in non-asbestos fiber reinforced friction materials—a review, Polymer composites, 18 (1997) 378-396.
[31] K. Friedrich, Friction and wear of polymer composites, Elsevier, 2012.

[32] C.J. Schwartz, S. Bahadur, S.K. Mallapragada, Effect of crosslinking and Pt–Zr quasicrystal fillers on the mechanical properties and wear resistance of UHMWPE for use in artificial joints, Wear, 263 (2007) 1072-1080.

[33] K. Plumlee, C.J. Schwartz, Improved wear resistance of orthopaedic UHMWPE by reinforcement with zirconium particles, Wear, 267 (2009) 710-717.

[34] C. Shoufan, L. Hongtao, G. Shirong, W. Gaofeng, Mechanical and tribological behaviors of UHMWPE composites filled with basalt fibers, Journal of Reinforced Plastics and Composites, 30 (2011) 347-355.
[35] X. Dangsheng, Friction and wear properties of UHMWPE composites reinforced with carbon fiber, Mater Lett, 59 (2005) 175-179.

[36] C. Liu, L. Ren, R.D. Arnell, J. Tong, Abrasive wear behavior of particle reinforced ultrahigh molecular weight polyethylene composites, Wear, 225-229 (1999) 199-204.

[37] Q. Wang, J. Liu, S. Ge, Study on Biotribological Behavior of the Combined Joint of CoCrMo and UHMWPE/BHA Composite in a Hip Joint Simulator, Journal of Bionic Engineering, 6 (2009) 378-386.

[38] L. Fang, Y. Leng, P. Gao, Processing of hydroxyapatite reinforced ultrahigh molecular weight polyethylene for biomedical applications, Biomaterials, 26 (2005) 3471-3478.

[39] C.H. Navarro, K.J. Moreno, A. Chávez-Valdez, F. Louvier-Hernández, J.S. García-Miranda, R. Lesso, A. Arizmendi-Morquecho, Friction and wear properties of poly(methyl methacrylate)–hydroxyapatite hybrid coating on UHMWPE substrates, Wear, 282-283 (2012) 76-80.

[40] S. Ge, S. Wang, X. Huang, Increasing the wear resistance of UHMWPE acetabular cups by adding natural biocompatible particles, Wear, 267 (2009) 770-776.

[41] W.J. Wood, R.G. Maguire, W.H. Zhong, Improved wear and mechanical properties of UHMWPE–carbon nanofiber composites through an optimized paraffin-assisted melt-mixing process, Composites Part B: Engineering, 42 (2011) 584-591.

[42] Y. Chen, Y. Qi, Z. Tai, X. Yan, F. Zhu, Q. Xue, Preparation, mechanical properties and biocompatibility of graphene oxide/ultrahigh molecular weight polyethylene composites, European Polymer Journal, 48 (2012) 1026-1033.

[43] S. Suñer, R. Joffe, J.L. Tipper, N. Emami, Ultra high molecular weight polyethylene/graphene oxide nanocomposites: Thermal, mechanical and wettability characterisation, Composites Part B: Engineering, 78 (2015) 185-191.

[44] Y.-S. Zoo, J.-W. An, D.-P. Lim, D.-S. Lim, Effect of Carbon Nanotube Addition on Tribological Behavior of UHMWPE, Tribology Letters, 16 (2004) 305-309.

[45] Y. Xue, W. Wu, O. Jacobs, B. Schädel, Tribological behaviour of UHMWPE/HDPE blends reinforced with multi-wall carbon nanotubes, Polymer Testing, 25 (2006) 221-229.

[46] D. Xiong, J. Lin, D. Fan, Wear properties of nano-Al2O3/UHMWPE composites irradiated by gamma ray against a CoCrMo alloy, Biomedical Materials, 1 (2006) 175.

[47] Y. Liu, S.K. Sinha, Wear performances and wear mechanism study of bulk UHMWPE composites with nacre and CNT fillers and PFPE overcoat, Wear, 300 (2013) 44-54.

[48] N. Satyanarayana, S.K. Sinha, B.H. Ong, Tribology of a novel UHMWPE/PFPE dual-film coated onto Si surface, Sensors and Actuators A: Physical, 128 (2006) 98-108.

[49] J.T. Burwell, Survey of possible wear mechanisms, Wear, 1 (1957) 119-141.

[50] J.K. Lancaster, Abrasive wear of polymers, Wear, 14 (1969) 223-239.

[51] H. Unal, U. Sen, A. Mimaroglu, Abrasive wear behaviour of polymeric materials, Materials & design, 26 (2005) 705-710.

[52] N.K. Myshkin, M.I. Petrokovets, A.V. Kovalev, Tribology of polymers: Adhesion, friction, wear, and mass-transfer, Tribology International, 38 (2005) 910-921.

[53] G. Deli, X. Qunji, W. Hongli, Physical models of adhesive wear of polytetrafluoroethylene and its composites, Wear, 147 (1991) 9-24.

[54] B.J. Briscoe, S.K. Sinha, Wear of polymers, Proceedings of the Institution of Mechanical Engineers, Part J: Journal of Engineering Tribology, 216 (2002) 401-413.

[55] M. Omar, A. Atkins, J. Lancaster, The role of crack resistance parameters in polymer wear, Journal of Physics D: Applied Physics, 19 (1986) 177.

[56] K. Friedrich, J. Karger-Kocsis, Z. Lu, Effects of steel counterface roughness and temperature on the friction and wear of PE(E)K composites under dry sliding conditions, Wear, 148 (1991) 235-247.

[57] T.B. Kirk, G.W. Stachowiak, A.W. Batchelor, Fractal parameters and computer image analysis applied to wear particles isolated by ferrography, Wear, 145 (1991) 347-365.

[58] F. Lockwood, R. Dalley, Lubricant analysis, ASM International, ASM Handbook, 18 (1992) 299-312.

[59] P.A. Williams, I.C. Clarke, Understanding polyethylene wear mechanisms by modeling of debris size distributions, Wear, 267 (2009) 646-652.

[60] M.Q. Zhang, Z.P. Lu, K. Friedrich, On the wear debris of polyetheretherketone: fractal dimensions in relation to wear mechanisms, Tribology international, 30 (1997) 87-102.

[61] B.J. Roylance, S. Raadnui, The morphological attributes of wear particles — their role in identifying wear mechanisms, Wear, 175 (1994) 115-121.

[62] G.P. Stachowiak, G.W. Stachowiak, P. Podsiadlo, Automated classification of wear particles based on their surface texture and shape features, Tribology International, 41 (2008) 34-43.

[63] A. Kobayashi, W. Bonfield, Y. Kadoya, T. Yamac, M. Freeman, G. Scott, P. Revell, The size and shape of particulate polyethylene wear debris in total joint replacements, Proceedings of the Institution of Mechanical Engineers, Part H: Journal of Engineering in Medicine, 211 (1997) 11-15.

[64] K. Friedrich, Z. Zhang, A.K. Schlarb, Effects of various fillers on the sliding wear of polymer composites, Composites Science and Technology, 65 (2005) 2329-2343.

[65] J.K. Lancaster, Material-specific wear mechanisms: relevance to wear modelling, Wear, 141 (1990) 159-183.

[66] T. Blanchet, F. Kennedy, Sliding wear mechanism of polytetrafluoroethylene (PTFE) and PTFE composites, Wear, 153 (1992) 229-243.

[67] Y. Wang, F. Yan, A study on tribological behaviour of transfer films of PTFE/bronze composites, Wear, 262 (2007) 876-882.

[68] C.J. Schwartz, S. Bahadur, Studies on the tribological behavior and transfer film-counterface bond strength for polyphenylene sulfide filled with nanoscale alumina particles, Wear, 237 (2000) 261-273.

[69] C.J. Schwartz, S. Bahadur, The role of filler deformability, filler-polymer bonding, and counterface material on the tribological behavior of polyphenylene sulfide (PPS), Wear, 251 (2001) 1532-1540.

[70] A. Sirota, On Abrasive Wear Resistance Dependence on the Molecular Characteristics of HDPE, Trenie I. Iznos, 7 (1986) 358-361.

[71] K. Marcus, C. Allen, The sliding wear of ultrahigh molecular weight polyethylene in an aqueous environment, Wear, 178 (1994) 17-28.

[72] H.J. Cho, W.J. Wei, H.C. Kao, C.K. Cheng, Wear behavior of UHMWPE sliding on artificial hip arthroplasty materials, Materials Chemistry and Physics, 88 (2004) 9-16.

[73] A. Essner, G. Schmidig, A. Wang, The clinical relevance of hip joint simulator testing: In vitro and in vivo comparisons, Wear, 259 (2005) 882-886.

[74] C.H. da Silva, A. Sinatora, Development of severity parameter for wear study of thermoplastics, Wear, 263 (2007) 957-964.

[75] A. Wang, A. Essner, C. Stark, J.H. Dumbleton, Comparison of the size and morphology of UHMWPE wear debris produced by a hip joint simulator under serum and water lubricated conditions, Biomaterials, 17 (1996) 865-871.

[76] W. Shi, H. Dong, T. Bell, Tribological behaviour and microscopic wear mechanisms of UHMWPE sliding against thermal oxidation-treated Ti6Al4V, Materials Science and Engineering: A, 291 (2000) 27-36.

[77] A. Wang, C. Stark, J.H. Dumbleton, Role of cyclic plastic deformation in the wear of UHMWPE acetabular cups, Journal of Biomedical Materials Research Part A, 29 (1995) 619-626.

[78] J.M. Dowling, D. Dowson, J. Charnley, The characteristics of acetabular cups worn in the human body, Bone & Joint Journal, 60 (1978) 375-382.

[79] J. Zhou, K. Komvopoulos, Wear mechanisms of untreated and gamma irradiated ultra-high molecular weight polyethylene for total joint replacements, ASME/STLE 2004 International Joint Tribology Conference, American Society of Mechanical Engineers, 2004, pp. 1767-1773.

[80] J. Tamura, I.C. Clarke, K. Kawanabe, M. Akagi, V.D. Good, P.A. Williams, T. Masaoka, D. Schroeder, H. Oonishi, Micro-wear patterns on UHMWPE tibial inserts in total knee joint simulation, Journal of Biomedical Materials Research Part A, 61 (2002) 218-225.

[81] C. McNie, D. Barton, E. Ingham, J. Tipper, J. Fisher, M. Stone, The prediction of polyethylene wear rate and debris morphology produced by microscopic asperities on femoral heads, Journal of Materials Science: Materials in Medicine, 11 (2000) 163-174.

[82] H. Unal, A. Mimaroglu, Friction and wear behaviour of unfilled engineering thermoplastics, Materials & Design, 24 (2003) 183-187.

[83] H.-C. Kuo, M.-C. Jeng, Dry Sliding Wear Properties of Ultra-high Molecular Weight Polyethylene Parts Made by the Injection Molding Process, Polymer-Plastics Technology and Engineering, 50 (2011) 604-612.

[84] O. Kulikov, K. Hornung, A simple way to suppress surface defects in the processing of polyethylene, Journal of Non-Newtonian Fluid Mechanics, 124 (2004) 103-114.

[85] A. Schallamach, How does rubber slide?, Wear, 17 (1971) 301-312.

[86] J. Wang, F. Yan, Q. Xue, Friction and Wear Behavior of Ultra-High Molecular Weight Polyethylene Sliding Against GCr15 Steel and Electroless Ni–P Alloy Coating Under the Lubrication of Seawater, Tribology Letters, 35 (2009) 85-95.

[87] J.H. Dieterich, Time-dependent friction and the mechanics of stick-slip, pure and applied geophysics, 116 (1978) 790-806.

[88] J.F.H. Archard, W. , The wear of metals under unlubricated conditions, Proceedings of the Royal Society of London. Series A. Mathematical and Physical Sciences, 236 (1956) 397.

[89] S. Ratner, I. Farberova, O. Radyukevich, E. Lure, Connection between wear resistance of plastics and other mechanical properties, Soviet Plastics, 7 (1964) 37-45.

[90] B.J. Briscoe, S. Sinha, Wear of polymers, Proceedings of the Institution of Mechanical Engineers, Part J: Journal of Engineering Tribology, 216 (2002) 401-413.

[91] V. Jain, S. Bahadur, Development of a wear equation for polymer-metal sliding in terms of the fatigue and topography of the sliding surfaces, Wear, 60 (1980) 237-248.

[92] I. Kraghelsky, E. Nepomnyashchi, Fatigue wear under elastic contact conditions, Wear, 8 (1965) 303-319.

[93] S.K.R. Chowdhury, P. Chakraborti, Prediction of Polymer Wear—An Analytical Model and Experimental Validation, Tribology Transactions, 51 (2008) 798-809.

[94] N. Viswanath, D.G. Bellow, Development of an equation for the wear of polymers, Wear, 181 (1995) 42-49.

[95] H.C. Meng, K.C. Ludema, Wear models and predictive equations: their form and content, Wear, 181 (1995) 443-457.

[96] A. Godest, M. Beaugonin, E. Haug, M. Taylor, P. Gregson, Simulation of a knee joint replacement during a gait cycle using explicit finite element analysis, Journal of biomechanics, 35 (2002) 267-275.

[97] R.K. Korhonen, A. Koistinen, Y.T. Konttinen, S.S. Santavirta, R. Lappalainen, The effect of geometry and abduction angle on the stresses in cemented UHMWPE acetabular cups–finite element simulations and experimental tests, Biomedical engineering online, 4 (2005) 32.

[98] T.A. Maxian, T.D. Brown, D.R. Pedersen, J.J. Callaghan, A sliding-distance-coupled finite element formulation for polyethylene wear in total hip arthroplasty, Journal of biomechanics, 29 (1996) 687-692.

[99] T. Ingrassia, L. Nalbone, V. Nigrelli, D. Tumino, V. Ricotta, Finite element analysis of two total knee joint prostheses, International Journal on Interactive Design and Manufacturing (IJIDeM), 7 (2013) 91-101.

[100] N. Suhendra, G. Stachowiak, Computational model of asperity contact for the prediction of UHMWPE mechanical and wear behaviour in total hip joint replacements, Tribology Letters, 25 (2007) 9-22.

[101] M. Mirghany, Z. Jin, Prediction of scratch resistance of cobalt chromium alloy bearing surface, articulating against ultra-high molecular weight polyethylene, due to

third-body wear particles, Proceedings of the Institution of Mechanical Engineers, Part H: Journal of Engineering in Medicine, 218 (2004) 41-50.

[102] M. Solar, H. Meyer, C. Gauthier, C. Fond, O. Benzerara, R. Schirrer, J. Baschnagel, Mechanical behavior of linear amorphous polymers: Comparison between molecular dynamics and finite-element simulations, Physical Review E, 85 (2012).

[103] A. Moyassari, H. Mostafavi, T. Gkourmpis, M.S. Hedenqvist, U.W. Gedde, F. Nilsson, Simulation of semi-crystalline polyethylene: Effect of short-chain branching on tie chains and trapped entanglements, Polymer, 72 (2015) 177-184.

[104] T. Kavassalis, P. Sundararajan, A molecular-dynamics study of polyethylene crystallization, Macromolecules, 26 (1993) 4144-4150.

[105] M.J. Ko, N. Waheed, M.S. Lavine, G.C. Rutledge, Characterization of polyethylene crystallization from an oriented melt by molecular dynamics simulation, The Journal of chemical physics, 121 (2004) 2823-2832.

[106] M.S. Lavine, N. Waheed, G.C. Rutledge, Molecular dynamics simulation of orientation and crystallization of polyethylene during uniaxial extension, Polymer, 44 (2003) 1771-1779.

[107] J.M. Kim, R. Locker, G.C. Rutledge, Plastic deformation of semicrystalline polyethylene under extension, compression, and shear using molecular dynamics simulation, Macromolecules, 47 (2014) 2515-2528.

[108] I.-C. Yeh, J.W. Andzelm, G.C. Rutledge, Mechanical and structural characterization of semicrystalline polyethylene under tensile deformation by molecular dynamics simulations, Macromolecules, 48 (2015) 4228-4239.

[109] Y. Li, S. Wang, Q. Wang, A molecular dynamics simulation study on enhancement of mechanical and tribological properties of polymer composites by introduction of graphene, Carbon, 111 (2017) 538-545.

[110] A.R. Alian, M.A.N. Dewapriya, S.A. Meguid, Molecular dynamics study of the reinforcement effect of graphene in multilayered polymer nanocomposites, Materials & Design, 124 (2017) 47-57.

[111] Y. Li, S. Wang, Q. Wang, M. Xing, Molecular dynamics simulations of tribology properties of NBR (Nitrile-Butadiene Rubber)/carbon nanotube composites, Composites Part B: Engineering, 97 (2016) 62-67.

[112] L. Dai, V. Sorkin, Z. Sha, Q. Pei, P. Branicio, Y. Zhang, Molecular dynamics simulations on the frictional behavior of a perfluoropolyether film sandwiched between diamond-like-carbon coatings, Langmuir, 30 (2014) 1573-1579.

[113] S. Spiegelberg, A. Kozak, G. Braithwaite, Characterization of physical, chemical, and mechanical properties of UHMWPE, UHMWPE Biomaterials Handbook (Third Edition), Elsevier, 2015, pp. 531-552.

[114] G. Meinel, A. Peterlin, Plastic deformation of polyethylene II. Change of mechanical properties during drawing, Journal of Polymer Science Part A-2: Polymer Physics, 9 (1971) 67-83.

[115] A. Galeski, Z. Bartczak, A. Argon, R. Cohen, Morphological alterations during texture-producing plastic plane strain compression of high-density polyethylene, Macromolecules, 25 (1992) 5705-5718.

[116] C. G'Sell, A. Dahoun, Evolution of microstructure in semi-crystalline polymers under large plastic deformation, Materials Science and Engineering: A, 175 (1994) 183-199.

[117] J.S. Bergström, S.M. Kurtz, C.M. Rimnac, A.A. Edidin, Constitutive modeling of ultra-high molecular weight polyethylene under large-deformation and cyclic loading conditions, Biomaterials, 23 (2002) 2329-2343.

[118] M. Jasty, D.D. Goetz, C.R. Bragdon, K.R. Lee, A.E. Hanson, J.R. Elder, W.H. Harris, Wear of polyethylene acetabular components in total hip arthroplasty. An analysis of one hundred and twenty-eight components retrieved at autopsy or revision operations, JBJS, 79 (1997) 349-358.

[119] R.S. Pascaud, W.T. Evans, P.J.J. McCullagh, D. Fitzpatrick, Critical assessment of methods for evaluating JIC for a medical grade ultra high molecular weight polyethylene, Polymer Engineering & Science, 37 (1997) 11-17.

2. INVESTIGATING UHMWPE WEAR MECHANISMS BY DECOMPOSING WEAR DEBRIS DISTRIBUTIONS[1]

2.1 Introduction

As two mating parts move in relation to each other, the result is energy loss (friction) and material loss in the form of wear debris. In order to make longer lasting, more efficient components, the wear processes involved at these contacts must be understood. Studying the wear mechanisms *in situ* is very difficult, so other techniques must be applied to gain information. It has been shown that the resultant wear debris reveals a great deal of information on the wear processes [1].

Ferrography in particular has been successful in classifying metallic debris in terms of size and shape, and then correlating these factors to specific wear mechanisms [2-4]. Since many shapes found in natural phenomena are complex, fractal analysis can also applied to describe to the complexity of the shape [2, 5, 6]. One common fractal analysis technique is the Richardson method, which describes how the perimeter of a particle varies over different size scales.

Polymers are widely used as bearing materials within the aerospace and aviation industries due to their light weight, low friction, and low noise levels. Other polymers, such as ultra-high molecular weight polyethylene (UHMWPE), have been used in

---

[1] Originally published as: K. Plumlee, C. Schwartz, Investigating UHMWPE wear mechanisms by decomposing wear debris distributions, Wear, 271 (2011) 2208-2212.

biomedical applications, such as artificial joints, due to its low wear and chemical inertness within the body. Understanding the tribologic behavior of such polymers has proven challenging in many cases; however, the analysis techniques developed for metallic components may be useful for characterizing polymeric wear.

Although UHMWPE wear debris has been studied extensively due to its involvement in the osteolytic process in artificial joints [7], UHMWPE wear processes are only partially understood and much debated. It is generally accepted that there are multiple processes at work, including adhesion, abrasion, fatigue, and viscoelastic behavior. Williams et al demonstrated that the total UHMWPE debris distribution is best described as a summation of multiple smaller distributions [8]. Williams attributed this to the presence of multiple wear mechanisms, but did not assign any particular region to any particular behavior. Zhang *et al* had success at applying analysis techniques similar to the methods used on metals to classifying polyether ether ketone (PEEK) debris [6]. PEEK is a common tribologic polymer, and has a high melting temperature and high stiffness. UHMWPE is a softer, more elastic polymer, and therefore has distinctly different wear processes.

This study aims to prove that UHMWPE debris can be characterized by tailoring previously established techniques towards use on polymers. The resulting debris distributions can then be compared to existing wear processes seen in metals and other polymers for insight into specific wear mechanisms.

2.2 Materials and Methods

UHMWPE wear pins, 6.25 mm in diameter, were created via compression molding at 230°C and 100 MPa for 10 min. Prior to wear testing, the surface of each wear pin was smoothed using 800 grit abrasive paper. Wear testing was performed on a custom built, two-axis pin-on-plate tribometer. The wear pins traced out a 15mm square path on the counterface while under a loading of 3 MPa and traveling at 75 mm/sec. No lubrication was used. Three different counterface roughnesses were tested: 6.35 mm thick stainless steel plate (type 410, heat treated to 45 HRC) was polished to two different surface roughnesses, which will be referred to as smooth (0.15 μm Ra) and rough (0.5 μm Ra). The third configuration consisted of 400 grit, silicon carbide abrasive paper adhered to a steel plate. This resulted in a surface roughness of approximately 5.0 μm. These counterfaces are shown in Figure 1.

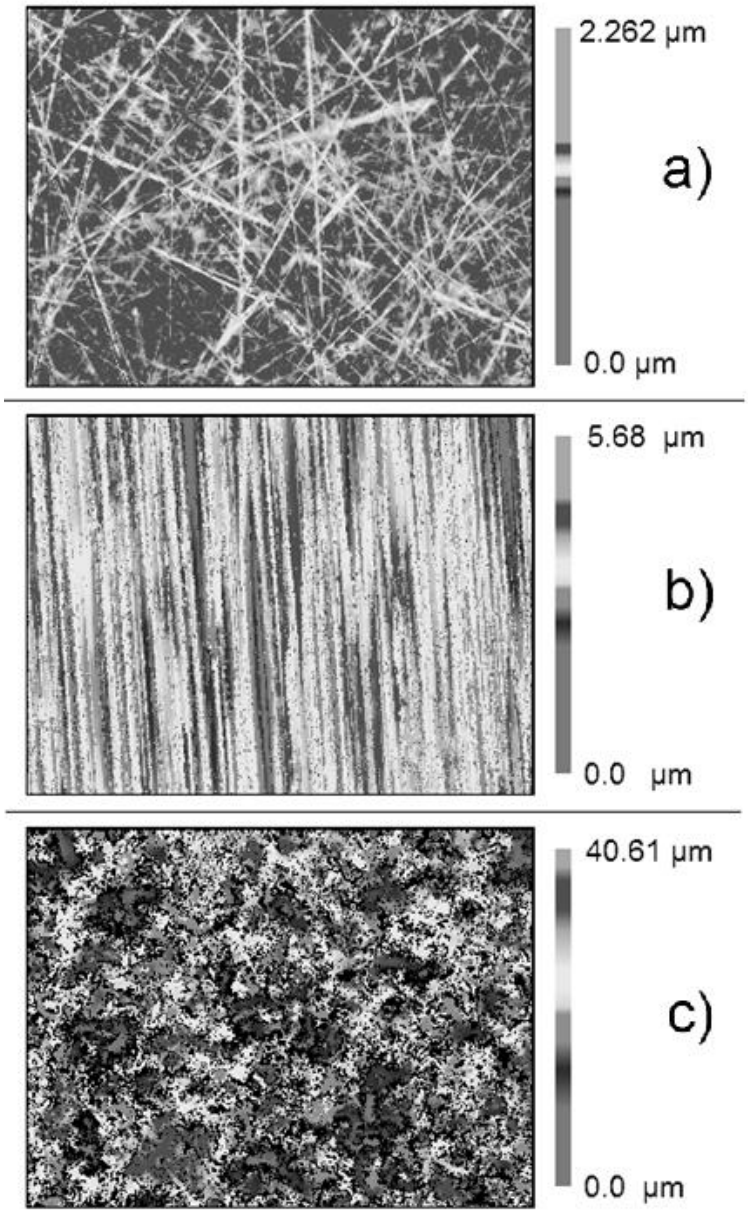

Figure 1: Surface plot of the three different counterfaces: a) smooth, b) rough, and c) abrasive paper

At the conclusion of a 100,000 cycle wear test, wear debris was collected by rinsing both the counterface and wear pin with isopropyl alcohol (IPA). The rinse fluids were then run through a density gradient created with IPA and distilled water. The wear

debris accumulated in a band within the density gradient, and that region was selectively collected using a pipette, and then run through on 0.1 μm filters (Millipore *Isopore* membrane filter). The filters were dried and gold sputter-coated, then images of the particles stuck on the filters were taken using a JOEL JSM-6400 scanning electron microscope.

Images of individual particles (non-agglomerates) were processed using image processing software to determine the outline and area of each particle, which was then analyzed for equivalent circle diameter (ECD) [9], roundness factor (RF) [4], and Richardson fractal number [2, 5, 6, 10]. While there are other descriptors used frequently in debris analysis, these three descriptors provide a cross-section of information. ECD is a measure of particle size, given as the diameter of a circle which would have the same area as the particle image (Eq. 1). Roundness factor is a measure of particle shape and is defined as the ratio of the perimeter squared over the area, all divided by 4π. This results in a value of one representing a perfect circle, while larger values represent more irregular shapes (Eq. 2).

$$\text{Equivalent Circle Diameter} = 2 * \sqrt{\text{Area}/\pi} \qquad \text{(Eq. 1)}$$

$$\text{Roundness factor} = \text{Perimeter}\text{\^{}}2/(\text{ Area} * 4 * \pi) \qquad \text{(Eq. 2)}$$

The Richardson fractal dimension, as seen in Figure 2, is a measure of perimeter complexity. Values typically range from 1.0, representing simple, straight borders to 1.4, which represents rough, fringed edges. To measure fractal dimension, each particle image was processed to define the particle boundary. The perimeter of each particle is then measured at different size scales by using different sized line segments. The numbers of segments that it takes to trace out the particle perimeter is recorded, along with the segment size. The segment size is then decreased, and the process is repeated. As the segment size decreases, more of the fine detail of the perimeter can be measured, thus leading to an increase in measured length. The perimeter measurements are then plotted against segment length on a log-log scale, and the fractal dimension is calculated as the slope of a linear best-fit approximation.

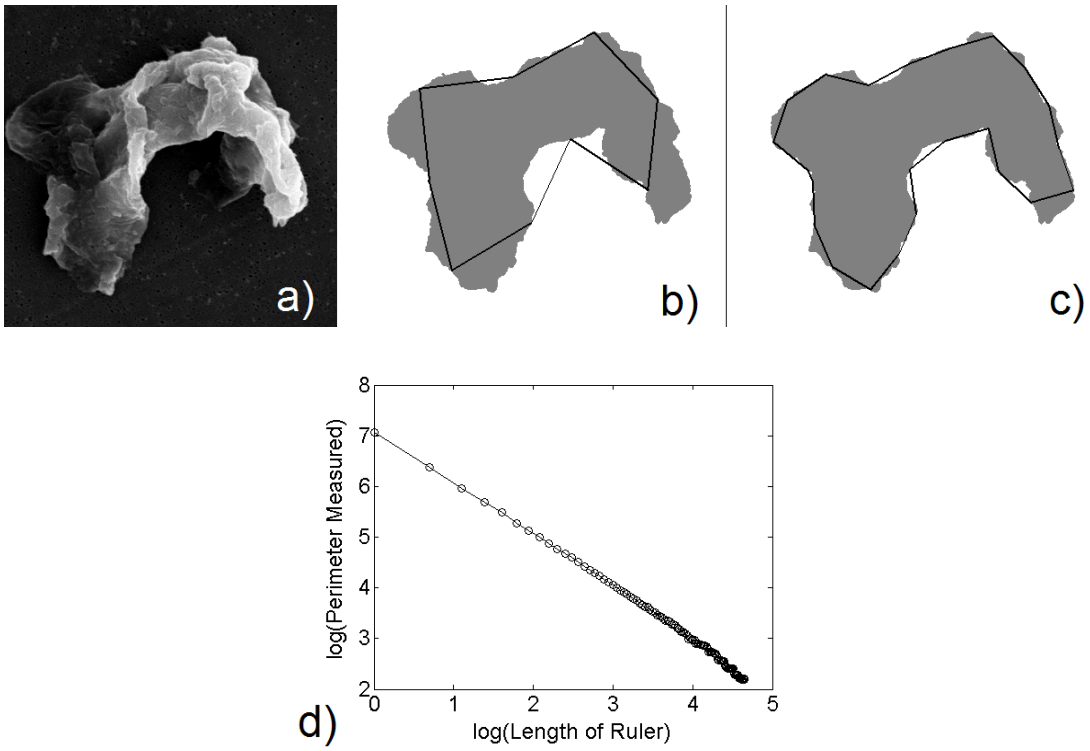

Figure 2: The Richardson fractal method: (a) Original particle image, (b) processed image with large segment size, (c) processed image with smaller segment size, and (d) log-log plot of perimeter data vs. ruler size.

2.3 Results and Discussion

Approximately 50 particles were analyzed for each of the counterface conditions (Fig 3). Distributions of the ECD, roundness factor, and fractal dimension are seen in the histograms below (Figs. 4-8).

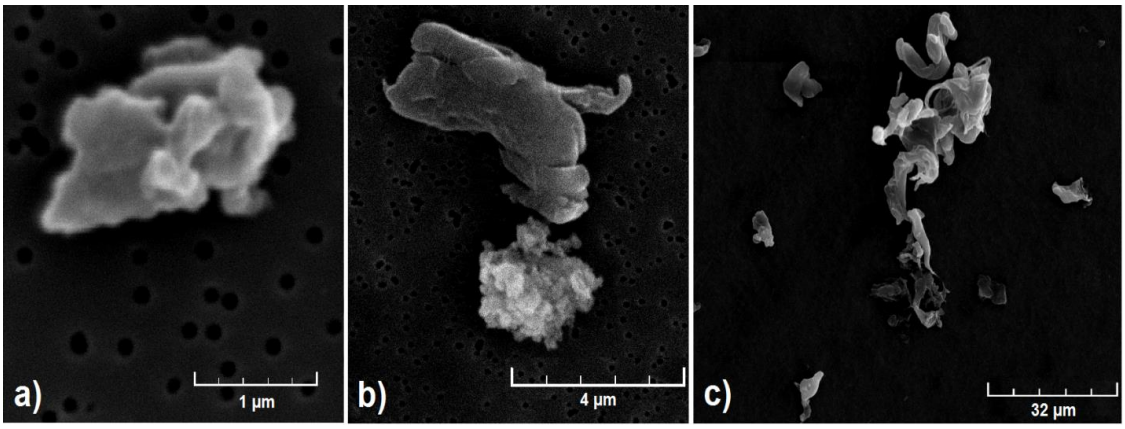

Figure 3: Example of wear particles collected from the (a) smooth counterface (ECD = 1.5 µm, RF = 3.32, FD = 1.08), (b) rough counterface (ECD = 3.2 µm, RF = 6.25, FD = 1.11), and (c) abrasive paper (ECD = 17.4 µm, RF = 16.0, FD = 1.20).

As expected, the distribution of particle size (as signified by the ECD) is influenced to a certain extent by counterface roughness [11, 12]. The smooth counterface had a narrow distribution of particles approximately centered around 1 µm, while the rough counterface had particles only slightly larger in size and with a wider distribution. These distributions match closely with previous literature [13]. It is also interesting to note that samples tested on the rough counterfaces lost four times as much mass as the smooth counterface samples.

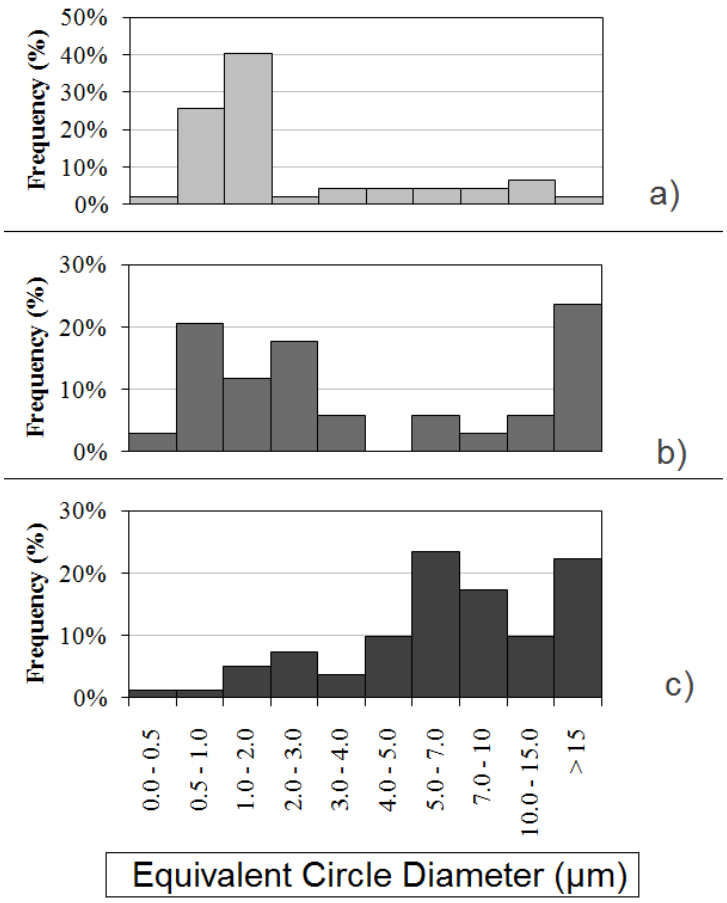

Figure 4: Histograms of Equivalent Circle Diameter (ECD) for each counterface: (a) smooth, (b) rough, and (c) abrasive paper.

While the abrasive paper yielded the largest particle size on average, all three counterfaces produced particles in the 30-40 µm range. It is suspected that many of the large particles formed early in the wear process, while the wear pin surface was not yet conformed to the counterface. Since the wear pins were relatively rough at the start of each test, there would be many regions of higher localized loads, as well as flakes and chips from the preliminary smoothing with abrasive paper that would be readily removed

early in the wear process (although the mechanisms of the removal may not be same in every case). It will be important to account for the break-in period in future testing.

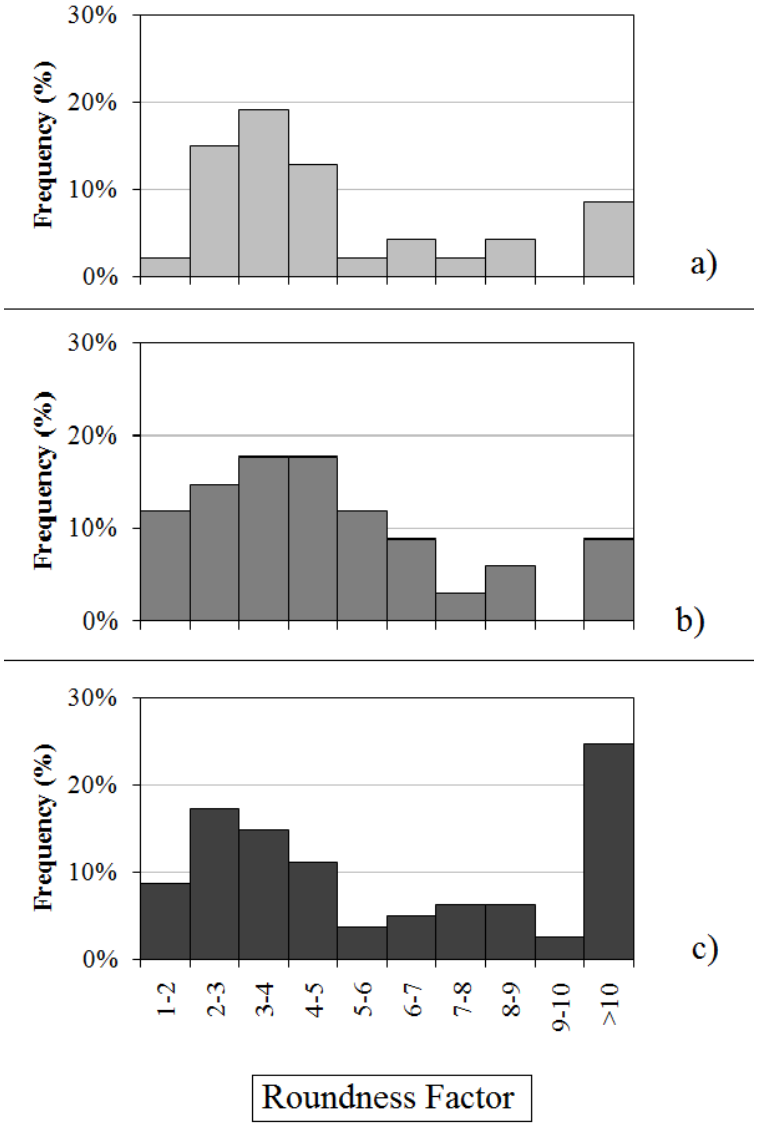

Figure 5: Histograms of Roundness Factor for each counterface: (a) smooth, (b) rough, and (c) abrasive paper.

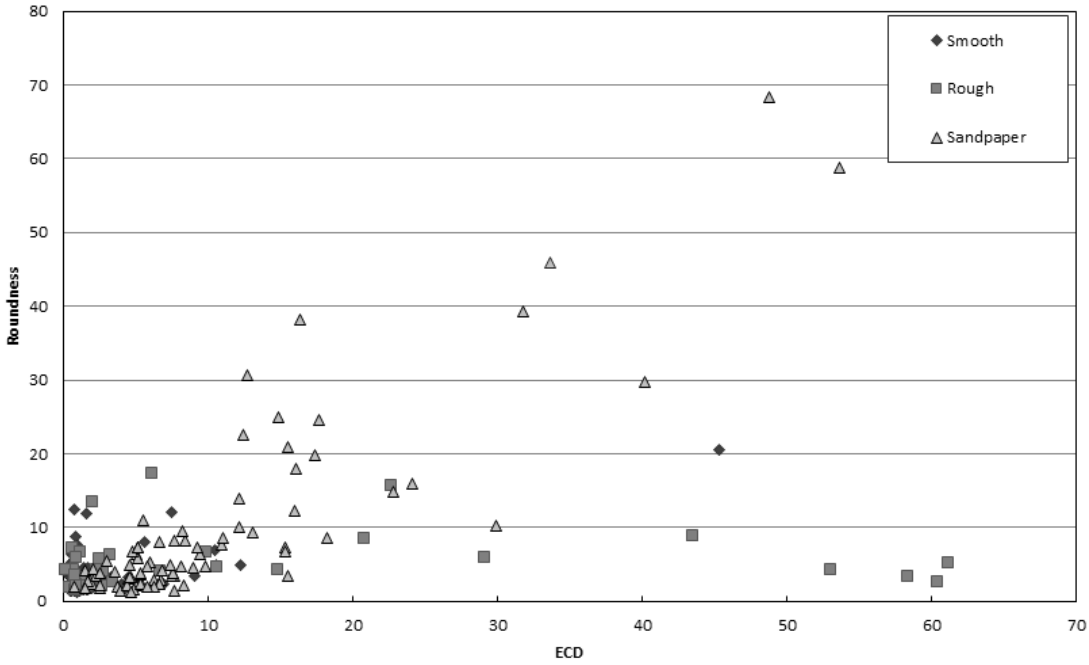

Figure 6: Roundness factor in relation to particle size (ECD)

Roundness factors between all three counterfaces were very similar, with the rough counterface producing a slightly wider distribution (Fig. 5). The abrasive paper produced more large particles that were jagged and irregularly shape, with the largest particles having the most irregular shapes. In previous studies dealing with metal particles, roundness factors above nine were associated with cutting processes [4]. This data range corresponds well to the larger particles, particularly from the abrasive paper counterface, suggesting that abrasive wear mechanisms formed those particular particles

Visually, there is an obvious difference between large particles from the abrasive paper counterface, which had roundness values over 10, and the large particles from the rough counterface which had roundness factor less than 10. When roundness factor is plotted against particle size, as seen in Figure 6, it becomes apparent that within the

abrasive paper-produced particles, the larger particles get more and more irregular. This trend was not seen in the other two counterfaces. This suggests that even though the steel counterfaces did produce a few particles of comparable size, it is unlikely they were generated by the same mechanism as the abrasive paper case.

This also suggests that excessively high roundness factors could be used as flag for highly abrasive wear within UHMWPE components. As the severity of the wear process increases, the particles become less rounded and more irregular.

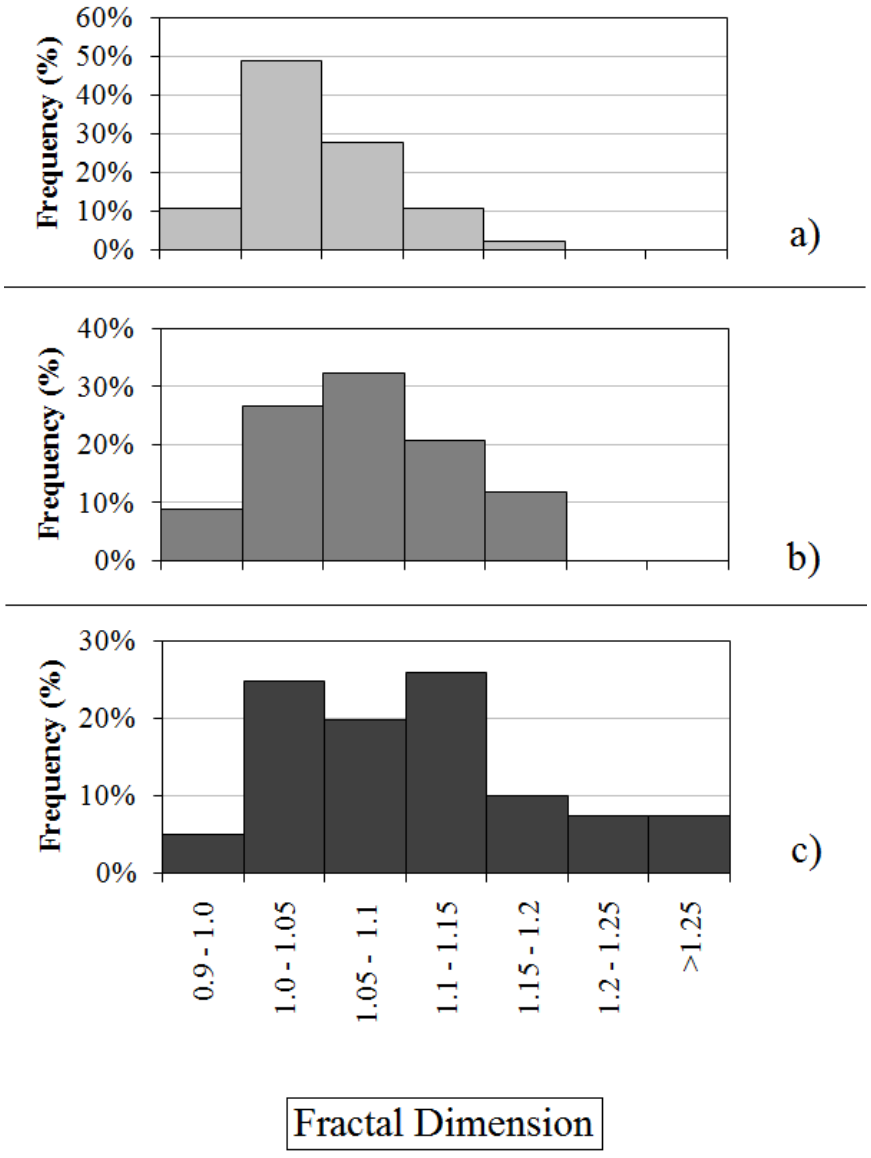

Figure 7: Histograms of Fractal Dimension for each counterface: (a) smooth, (b) rough, and (c) abrasive paper.

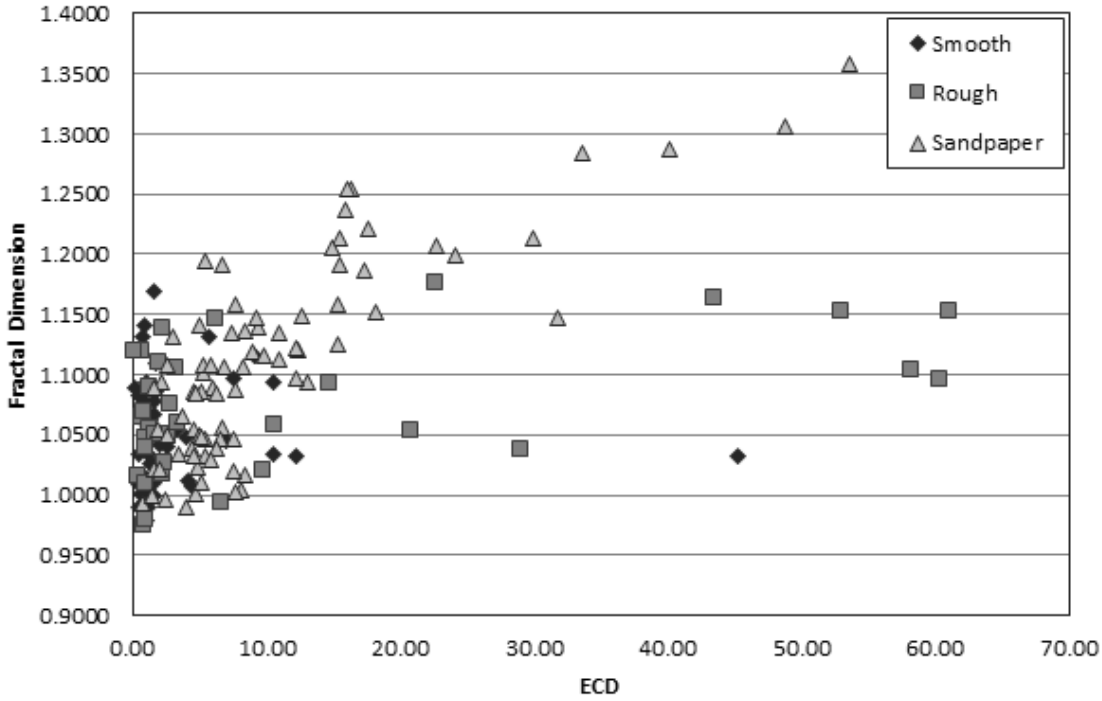

Figure 8: Fractal dimension in relation to particle size (ECD)

Particles produced from abrasive paper also showed the highest fractal dimension, with larger particles having larger fractal dimensions (Fig. 7 and 8). This trend was not demonstrated by debris from the other counterfaces. In a previous study, the fractal dimension of rubber debris created on a razor abrader ranged from 1.10 – 1.40, depending on the loading [10]. This corresponds very well with the larger particles found in the abrasive paper samples, reaffirming that these particles were formed during an abrasion process. This also suggests that the behavior of UHMWPE during this type of process is similar to elastic rubber behavior.

For all three counterfaces, there is a large group of particles that is not accounted for by the abrasion characteristics. These particles are fairly round in shape (RF less than

7) and have smooth outer boundaries (fractal dimensions between 1-1.07). Typically these particles have an ECD less than 10 μm, although there are exceptions. Of this group, a portion of particles appear to have a somewhat rough surface texture (Fig. 9a), suggesting a fracture surface generated by crack propagation. This supports the idea that along with abrasion, cyclic loading profiles promote crack propagation and fatigue-based wear. Upon visual inspection, these particles are similar to classic fatigue and pitting debris seen in metals, and have similar values in terms of roundness factor and fractal dimension. In this study, these particles typically had fractal dimensions between 1.04 and 1.07.

Other particles are very smooth looking, with no sign of a fracture surface (Fig. 9b). It is unclear if these particles are simply older "fatigue" particles, smoothed out after formation as they migrate away from the wear interface, or if they were formed by a separate formation process, such as viscoelastic flow under cyclic repetitive loading. These particles typically had fractal dimensions less than 1.05. However, the close proximity in terms of ECD, roundness factor, and fractal dimension to the "fatigue" particles made it difficult to distinguish between the two in this study. This could be improved with higher resolution images of small particles and increased sample populations.

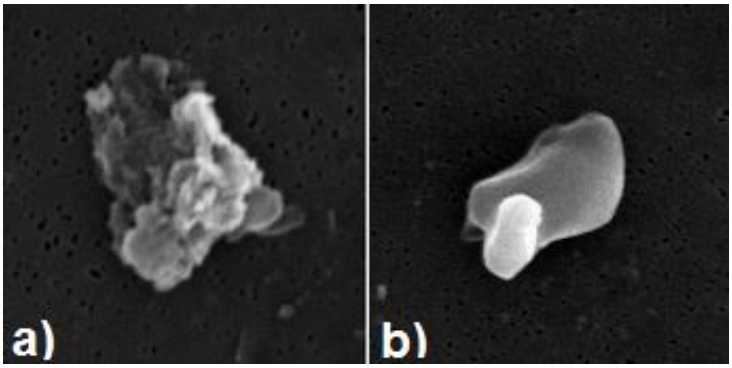

Figure 9: Wear debris generated on the smooth counterface. Both of comparable size, roundness factor, and fractal dimension; however, the textures are distinctly different.

2.4 Conclusions

Ultra-high molecular weight polyethylene experiences multiple wear mechanisms during sliding. Wear debris collected from UHMWPE bearings provided insight into the wear mechanisms. Classifying the debris in terms of equivalent circle diameter, roundness factor, and Richardson fractal dimension was used to identify debris produced from severe abrasion. The roundness factor and fractal dimension of the particles matched well with previously published results from both metal particles and other polymer based studies. Smaller particles that were not associated with abrasion were also identified. It is suspected that many of the particles result from fatigue processes, but other particles were of similar size but were distinctly smoother. It is unclear whether these are particles which have been smoothed out during their time trapped as third body debris, or if these particles are the result of an entirely different wear mechanism.

In future studies, it will be important to account for break-in periods for each wear pin, gather large sample populations, and take extra care should be taken during the imaging processing to get crisp images of the small particle boundaries. More developed

algorithms for analyzing particle texture, particularly away from the boundaries, could further distinguish particles for mechanism analysis.

2.5 References

[1] S. Jahanmir, Future Directions in Tribology Research, Journal of Tribology, 109 (1987) 207-211.

[2] T.B. Kirk, G.W. Stachowiak, A.W. Batchelor, Fractal parameters and computer image analysis applied to wear particles isolated by ferrography, Wear, 145 (1991) 347-365.

[3] F. Lockwood, R. Dalley, Lubricant Analysis, in: S. Henry (Ed.) ASM Handbook, ASM International, 1992, pp. 299-312.

[4] B.J. Roylance, S. Raadnui, The morphological attributes of wear particles -- their role in identifying wear mechanisms, Wear, 175 (1994) 115-121.

[5] P. Podsiadlo, G.W. Stachowiak, Scale-invariant analysis of wear particle surface morphology: II. Fractal dimension, Wear, 242 (2000) 180-188.

[6] M.Q. Zhang, Z.P. Lu, K. Friedrich, On the wear debris of polyetheretherketone: fractal dimensions in relation to wear mechanisms, Tribology international, 30 (1997) 87-102.

[7] J.H. Dumbleton, M.T. Manley, A.A. Edidin, A literature review of the association between wear rate and osteolysis in total hip arthroplasty, The Journal of Arthroplasty, 17 (2002) 649-661.

[8] P.A. Williams, I.C. Clarke, Understanding polyethylene wear mechanisms by modeling of debris size distributions, Wear, 267 (2009) 646-652.

[9] A. Kobayashi, W. Bonfield, Y. Kadoya, T. Yamac, M. Freeman, G. Scott, P. Revell, The size and shape of particulate polyethylene wear debris in total joint replacements, Proceedings of the Institution of Mechanical Engineers, Part H: Journal of Engineering in Medicine, 211 (1997) 11-15.

[10] P.R. Stupak, J.A. Donovan, Fractal analysis of rubber wear surfaces and debris, Journal of Materials Science, 23 (1988) 2230-2242.

[11] J.L. Hailey, E. Ingham, M. Stone, B.M. Wroblewski, J. Fisher, Ultra-high molecular weight polyethylene wear debris generated in vivo and in laboratory tests; the influence of counterface roughness, ARCHIVE: Proceedings of the Institution of Mechanical

Engineers, Part H: Journal of Engineering in Medicine 1989-1996 (vols 203-210), 210 (1996) 3-10.

[12] H. Sin, N. Saka, N.P. Suh, Abrasive wear mechanisms and the grit size effect, Wear, 55 (1979) 163-190.

[13] A. Galvin, J. Tipper, Nanometre size wear debris generated from crosslinked and non-crosslinked ultra high molecular weight polyethylene in artificial joints, Wear, 259 (2005) 977-983.

3. SURFACE LAYER PLASTIC DEFORMATION AS A MECHANISM FOR UHMWPE WEAR, AND ITS ROLE IN DEBRIS SIZE.[2]

3.1 Introduction

Polymers are commonly used in tribological applications due to their low coefficient of friction, low cost, and ease of manufacturing, but are often limited in terms of product lifespan. Additionally, recent studies have shown that the microscopic wear debris generated by polymer bearing materials can lead to adverse health effects in people [14-16]. While a significant portion of research has been directed towards reducing the overall wear on a bulk level, the complexity and subsequent lack of understanding of polymer wear mechanisms means that many of these techniques cannot address the formation of individual particles, and therefore the associated health concerns remain unaltered.

Ultra-high molecular weight polyethylene (UHMWPE) is a common tribological material used in orthopedic implants. The wear debris generated from these components is responsible for potentially catastrophic loosening of the implant through a process called osteolysis [7, 17]. The severity of this condition has led to a large quantity of research being performed on UHMWPE wear, including the development of wear reduction techniques such as crosslinking [18, 19] and the use of composite fillers [20-23]. Despite

---

[2] Originally published as: K.G. Plumlee, C.J. Schwartz, Surface layer plastic deformation as a mechanism for UHMWPE wear, and its role in debris size, Wear, 301 (2013) 257-263

the quantity of research, very little is known about the wear mechanisms of UHMWPE, in particular, how individual wear particles are formed. As a result, many of the techniques developed do not drastically reduce osteolytic response.

To gain the required insight into wear behaviors, there are two historical methods typically employed: the analysis of the resulting wear surface and the analysis of the debris geometry. Each method looks for specific markers that suggest particular behaviors, such as cracking, pitting, grooves, and scratches. In regards to UHMWPE, these methods have answered very few questions while generating many more. For example, debris analysis has revealed that UHMWPE likely experiences multiple wear mechanisms, and that the osteolytic response is most strongly tied to debris that is small ($\leq$ 1μm), round, and smooth; a class of particles that does not fit any known wear mechanism [24]. However, the smoothness of the particles suggests that plastic deformation plays a critical role. Also, the resultant wear surface of UHMWPE is extremely smooth, with very little cracking, pitting, or scratches, and the counterface does not collect a transfer film like many other notable tribologic polymers, such as PTFE. However, one notable surface feature has been repeatedly described: the formation of microscopic sinusoidal ripples across the wear surface (Fig. 10). In 1978, Charnley and Dowling, pioneers of the artificial hip, described the phenomenon: "The cause of the parallel ripples has not yet been identified," and commented that why the multi-direction behavior "should produce such an oriented topography is hard to explain" [25]. Over 30 years later, Wang *et al* commented on the same phenomena: "It is still not well understood how the ripples are formed...but it is

generally accepted that accumulated plastic deformation plays a critical role in the formation of the ripple-like features on the surface of the acetabular cups" [26].

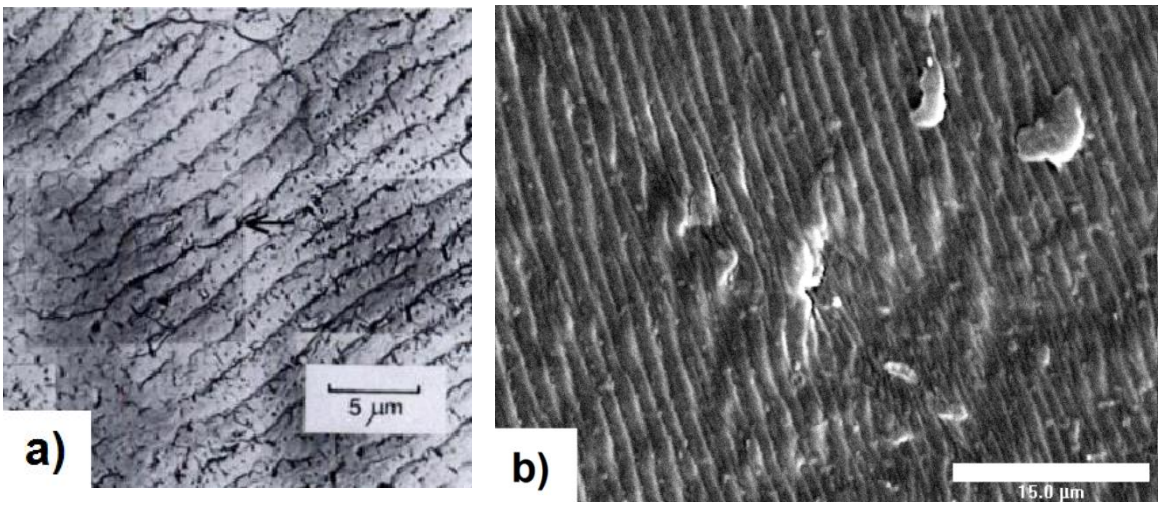

Figure 10: Ripple formation seen on UHMWPE wear surfaces. a) Reprinted from Dowling and Charnley [13], and b) ripples formed on the custom-built used in this study

To cultivate a new generation of innovative solutions for reducing both osteolytic response and wear in general, tribologists are seeking a better understanding of the wear mechanisms involved in UHMWPE, particularly regarding the role of plastic deformation. Recent efforts in computational modeling have provided support to the claim that plastic deformation accumulates at the surface, but these models assumed simplified geometries and material properties, and lacked any experimental verification of the results.

This study aims to expand the computational support for "plastic deformation" wear through application of realistic geometries and adhesive forces, and also to provide experimental support through the development of a novel surface-notch technique that provides a new tool in the arsenal of wear behavior analysis. Through these tests, a

theoretical model for the development of surface ripples is also derived, based on accumulated strain at the polymer surface.

3.2 Materials and Methods

All experimental work was conducted using UHMWPE samples (GUR-1050, Ticona) formed through compression molding. Wear tests were performed using cylindrical, UHMWPE wear pins, 6.25mm diameter, which traced 20mm diameter circles on a polished, stainless steel plate (type 410, heat treated to 45 HRC, polished to 0.05μm Ra). Wear tests were performed on a custom built, 2-axis wear simulator, and were performed under dry sliding conditions with normal loads of 3MPa and speeds of 200 mm/s.

Modeling was conducted using Abaqus software in conjunction with Texas A&M University's Supercomputing Facility. All simulations were performed using 2D models for solving efficiency. Initial simulations of the wear process were based upon the previous work of Suhendra and Stachowiak [27]. However, it is unclear if the slightly exaggerated asperity geometry used in their work is reflective of actual orthopedic wear when smoother asperity geometry may result in a more evenly distributed load, and therefore less plastic deformation. Also, when multiple asperities are close together, they may act as a single, blunt asperity rather than sharp points. To test these points, model geometries were generated from surface profiles taken from actual worn polymer and counterface wear surfaces obtained via a Zygo NewView 600 non-contact profilometer.

To confirm the presence of accumulated strain at the surface as evidenced by the simulations, a simple test was developed to reveal any changes in geometry after a wear process. In these tests, wear pins were pre-worn for 100,000 cycles using 20mm diameter circular path. At the conclusion, the smoothed wear pin surface was grooved using a fresh razor blade. The blade was drawn across the surface with minimal pressure, achieving a consistent triangular groove between 5μm and 10μm deep. These samples were then subjected to a variety of additional wear testing such that any plastic deformation at the pin surface would be reflected in the groove geometry. At the completion of the additional wear tests, the surface of the sample was sputtercoated with gold, then imaged in a scanning electron microscope (JOEL-6400).

3.3 Results and Discussion

3.3.1 Simulation

Abaqus simulations performed on imported geometry, multiple asperity model result in stress distributions that match well with expected results calculated using hertzian contact mechanics, and match well with the results from Suhendra and Stachowiak [27], despite the smoother asperity geometry. Contact areas were limited to the asperity peaks, and neighboring asperities were far enough apart that their corresponding stress distributions did not influence each other in the region that experiences deformation. When the model was loaded at an average pressure of 3MPa, which is under the yield strength of UHMWPE, the smooth surface still has sufficient asperity sharpness to cause concentrated stress distributions, and the stresses experienced are high enough to generate

yielding at the surface according to the Von Mises criterion, with peak loads in excess of 30 MPa (Fig 11a). The resulting plastic deformation is limited to a relatively thin layer at the surface, and is propagated along the surface as the asperities move across the surface (Fig. 11b). The depth of this deformed layer varied according to the local asperity geometry, but ranged from 100nm to 500nm, which also closely matches the theoretical depth of the maximum shear stress of approximately based on contact mechanics, which is approximately one-half the contact width, although discontinuities within the strain field as discussed by Suhundra and Stachowiak could result in even thinner regions.

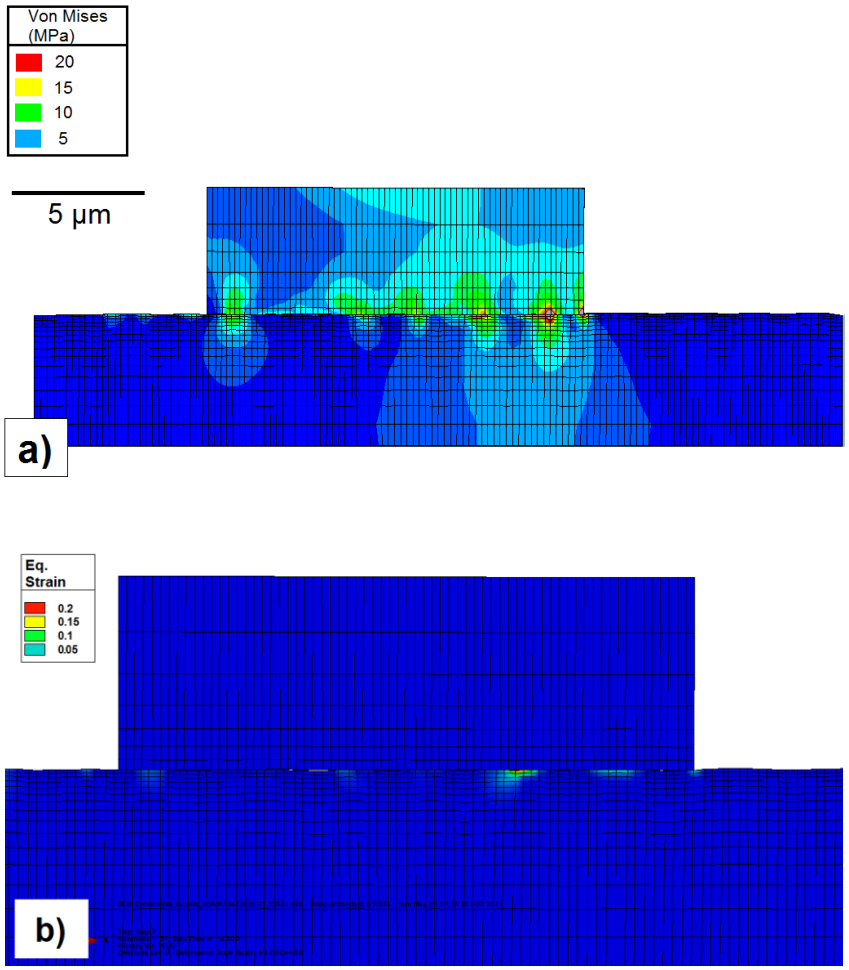

Figure 11: Abaqus results using imported surface profiles: a) Von Mises Stress, and b) Equivalent Plastic Strain

3.3.2 Grooved-Surface Test

To verify the presence of this plastically deformed surface layer in physical specimens, a novel grooved-surface test was developed. Initially, the razor blade grooves had very smooth edges and boundaries, as seen in Figure 12a. When a grooved sample was subjected to a linear wear path that ran in the same direction as the groove, no notable changes were evident in the groove, even after 40 cycles (Fig. 12b). However, when the direction of the wear path crossed the groove (both circular and linear-perpendicular paths were tested), distinct distortions in the groove boundaries were found. These alterations were evident in as few as a single cycle, adding support to the simulation results that demonstrated deformation in small number of asperity passes. The types of distortions observed could be categorized into three types: 1) bulging edges, 2) large overlying flakes, and 3) thin sheets and fingers, 1µm in thickness or less.

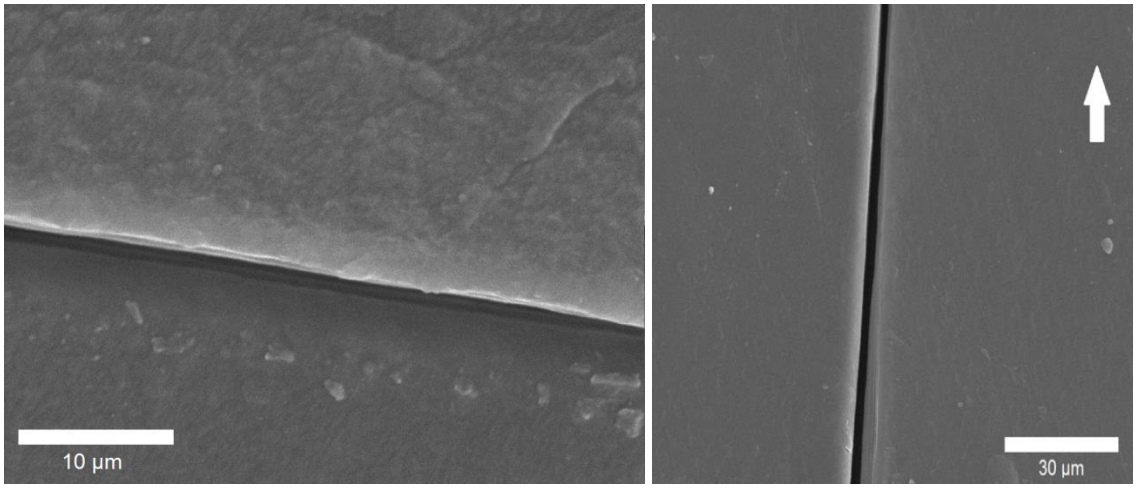

Figure 12: A razor blade makes a clean groove across a wear surface. a) the original groove with no additional wear, b) The groove remains clean in geometry after 40 cycles of additional wear in a linear direction parallel to the groove.

The *bulging edges* are hypothesized to be products of an imperfect razor blade grooving method, where the blade created excessively large raised lips along the sides of the groove as material was displaced (Fig. 13). These tall lips are then smoothed back into the groove once a wear test is begun. This produces a groove geometry that has bulged sizes, and is most evident when the grooving process was performed unsteadily or with too much pressure. Since these formations are products of the grooving process and not representative of a wear behavior, they are not relevant in this study.

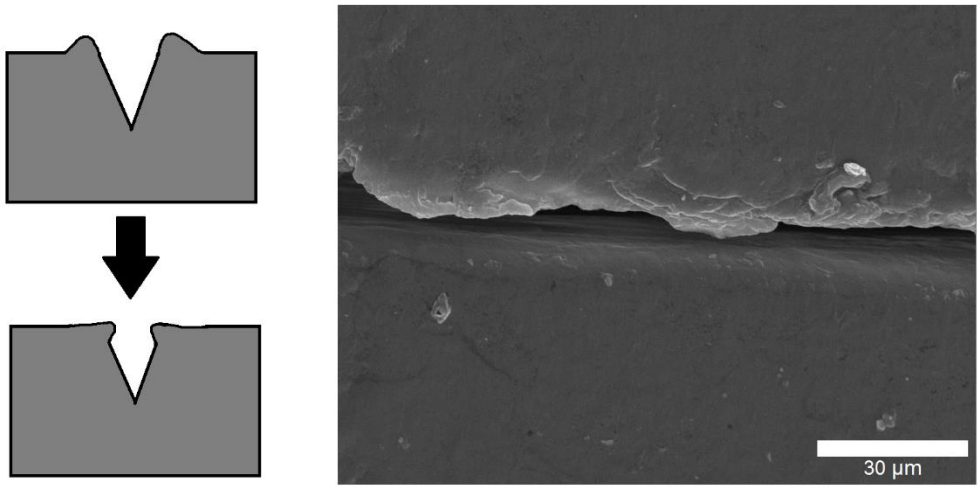

Figure 13: The tall lip on the sides of the groove that results from excessively deep grooving will fold back over the gap, masking other forms of deformation.

Although similar in appearance, the second groove distortion appears when wear debris migrates across the groove during the wear process, often bridging the entire groove width. These "free-floating" particles are typically large flakes with diameters of 10µm or greater and thickness in the 1-5µm range (Fig. 14a-c). Particles of similar shape and size have been noted in other investigations of UHMWPE wear behavior. It is interesting to note that for the dry sliding conditions of this experiment, these large flake-like particles were seen in significant numbers across the wear surface and appear to be smoothed against the bulk polymer, giving rise to their flat shape. The size and shape of these particles is very similar to the debris generated by polymers that create transfer films, such as PEEK and PTFE, although UHMWPE itself is not known for generating transfer films (Fig. 14d). Since particles of this sort are found only on the UHMWPE bulk and not found on the counterface, it is hypothesized that these particles are behaving as a weak transfer film that clings to the polymer bulk instead of the counterface. Expanding on this

hypothesis, it follows that these flakes can grow through the accretion of neighboring particles, similar to the growth of traditional transfer films through deposition of additional material. In this manner, these flake-like particles create a thin protective layer of deposited material that can deform and shift independent from the bulk, contributing to the low wear rate of UHMWPE. The strength of the bond between these particles and the polymer bulk is still unknown, but the migratory nature suggests these particles are not fully incorporated back into to the bulk polymer despite the smoothed appearance. These self-adhering transfer film flakes have been seen bridging grooves after only one cycle of motion.

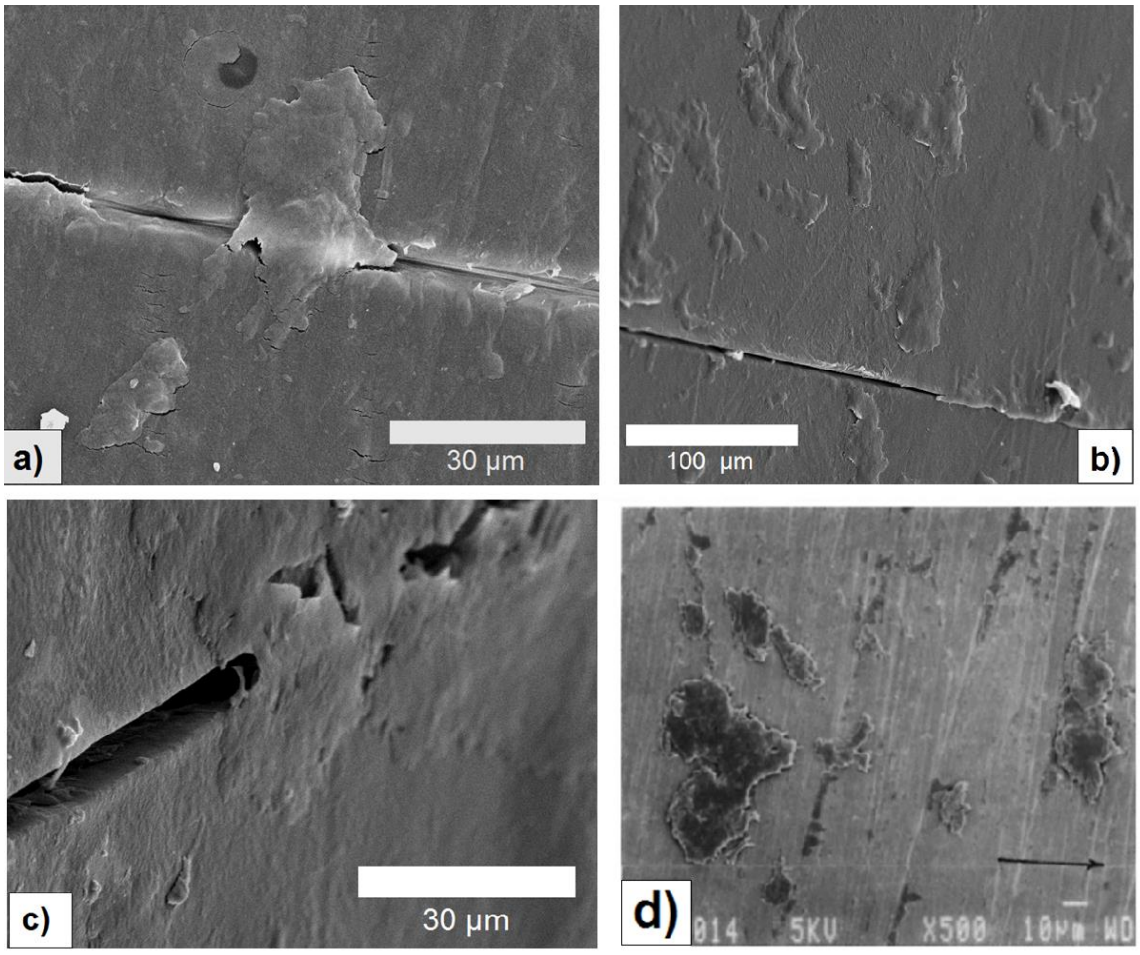

Figure 14: SEM Images of flake-like particles found attached to the polymer wear surface, bridging the groove. a) taken orthogonal to the surface, b) taken at 30° angle off vertical to show depth, c) taken at 60° off vertical, and d) images of PEEK transfer film deposited onto metal counterface, reprinted from Bahadur [19], which are similar in shape and texture to the UHMWPE particles.

The final type of distortions illuminated by the groove method is that of thin fingers and sheets drawn across the groove, as seen in Figure 15. These structures vary in width, but range in thickness from 0.05-0.5 μm, and have no surrounding structures that suggest they are portions of free-floating debris. Instead, the appearance suggests that a portion of the bulk surface has been pulled across the groove in a thin sheet. The thickness of these structures matches closely to the thickness of a plastically deformed layer as predicted by Abaqus simulations, and is also of the same size scale as the small, round debris particles that are strongly tied to osteolytic response in artificial joints. Additionally, as the number of cycles increases, the total width, but not the thickness, of these structures increases, suggesting that strain accumulates across the surface with each asperity pass, which is also shown in simulations. Over a sufficient number of cycles, entire regions of the groove can be covered with a thin polymer skin, as seen in Figure 1c.

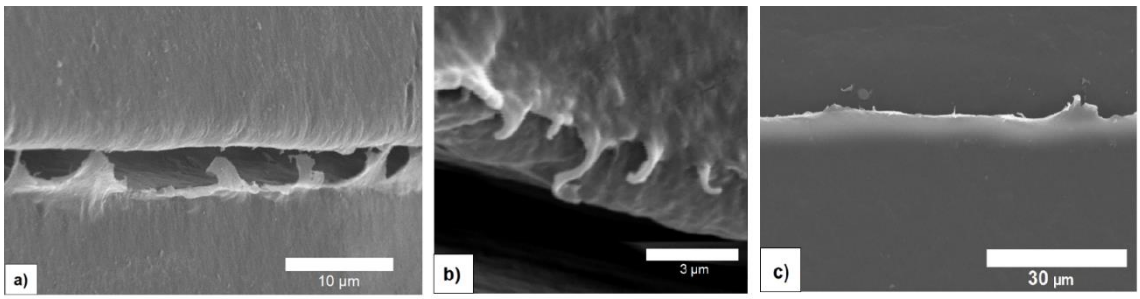

Figure 15: Images of thin sheets and fingers that are drawn across the groove. a) reveals the thickness of the plastically deformed layer is less than 1 μm, b) shows what may be

individual asperty pull out, and c) the eventual accumulation of strain leads to a thin sheet completely covering the groove, shown after 40 cycles**.**

3.3.3 Surface Geometry – Ripples

When plastic deformation is localized to a thin surface layer, as evidenced by both the simulation and experimental studies above, it provides theoretical rationale for the occurrence of the patterned surface ripples as commonly seen in UHMWPE wear components: the buckling of a polymeric thin film due to compression from its underlying soft substrate (Fig. 16).

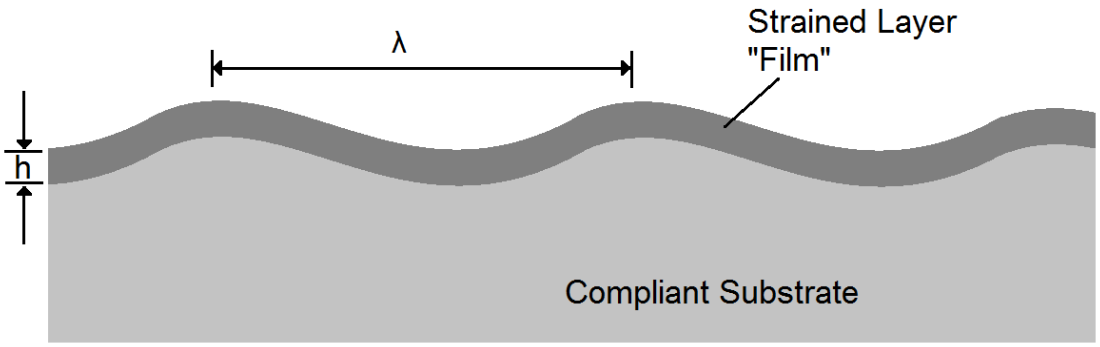

Figure 16: When subjected to compressive stress, a thin film bonded to a soft substrate will buckle into a sinusoidal pattern.

To simplify the rippling process, the strained surface layer is treated as a separate region from the bulk, but which remains strongly adhered to the bulk. Since the surface layer has undergone more strain more than the bulk, the bulk exerts a compressive stress on the layer as it "pulls" the thin film back towards its original position. A thin film undergoing compression will buckle when the compressive force exceeds a critical level. When this occurs, the final geometry for the system is dictated by the minimization of the energy of

three different elements: 1) the elastic energy stored in the stretched thin film region, 2) the bending energy stored in the thin film region, and 3) the deformation of the underlying bulk to match the film. The behavior of such systems, including the derivations of the energy equations that ultimately are used to predict geometry, have been studied extensively in other fields [28-30], and has been demonstrated in polymer-on-polymer films as seen in Figure 17. However, to the author's knowledge, this is the first time this approach has been applied to the phenomena seen in UHMWPE wear.

:

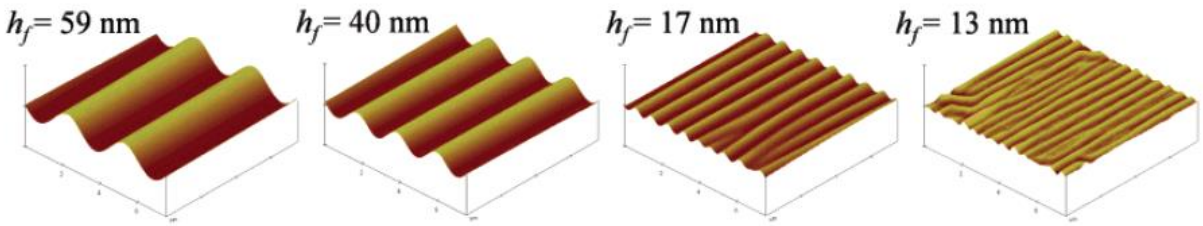

Figure 17: AFM images of the buckling of polystyrene film on a PDMS substrate, reprinted from Stafford [16].

In the case of a unidirectional stress state and an infinitely thick substrate, the resulting geometry follows a sinusoidal wave, with equilibrium wavelength, λ, given by:

$$\lambda = 2\pi h_f \left(\frac{\bar{E}_f}{3\bar{E}_s}\right)^{1/3}$$

where is h_f is the thickness of the deformed layer, $\bar{E} = E/(1-\nu^2)$ is the plane strain modulus, E is Young's modulus, ν is Poisson's ratio, and the subscripts *f* and *s* represent the deformed layer and substrate respectively. Note that the wavelength is only dependent on the moduli of the two layers and the film layer thickness, which is highly dependent on the modulus and yield strength of the polymer. The limited number of factors that influence ripple wavelength explains the relative consistency of ripple spacing throughout UHMWPE literature. As a general rule of thumb, assuming the two layers have roughly the same modulus and Poisson's ratio, the wavelength would be roughly $4.5h_f$, although the influence of strain-induced chain alignment will likely lead to an increase in film modulus and a subsequent increase in ripple spacing. Measurements taken from the grooved surface images discussed in section 3.2 revealed film thicknesses ranging from 0.05-0.5 μm, which correspond well to the ripple spacing as measured between 1.25-2.25 μm in this study.

It is anticipated that these models could also provide a range of possible ripple amplitudes based on the critical compressive stress required to initiate buckling and the maximum stress generated by the bulk, however, ripple height was not explicitly measured during this test, and this avenue was not pursued.

The formation of the sinusoidal ripples in the surface of UHMWPE affects debris formation in a number of ways. Firstly, it dictates the asperity geometry of the polymer surface, effectively dividing the surface contact area into small, discrete regions ≤1μm in width.

As the surface of the polymer is drawn laterally by the counterface, it is from the peaks of these ripples that material is removed, and the valleys of the ripples isolate each peak from each other, limiting the size of a single particle (Fig. 18). This size is strongly influenced by the deformed layer thickness, h_f, and the contact width. The shape of these particles would small and round, often having a slight tail from the drawing process.

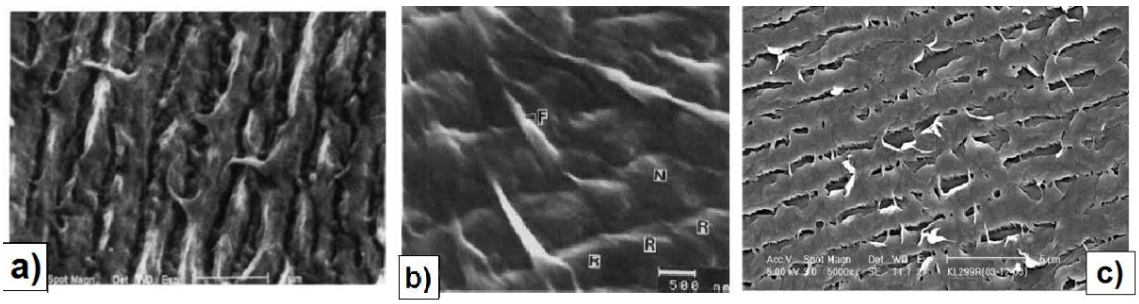

Figure 18: SEM images revealing continued plastic deformation and drawing originating from the peaks of the ripples. A) after being worn on a hip simulator, from Wang [14], b) worn on a hip simulator, from McKellop [20], and c) worn on a knee simulator from Asano [21].

Secondly, the rippled surface provides avenues of safety where small wear debris can settle and migrate, relatively free from the effects of the wear operation. Larger particles float across the surface of the ripples, where they are continually flattened and deformed by the counterface. These larger particles may absorb other particles, or break apart into smaller flake-like particles, creating a somewhat irregular shape. However, as long as their dimension is longer than the wavelength of the ripple spacing, they will remain flat and flake-like (Fig. 19a). For particles approximately the same dimension as the ripple amplitude and spacing, the ripples may act as initiators for rolling motion

instead of smearing across the surface, creating extremely smooth ovoid shaped particles as they tumble (Fig. 19b).

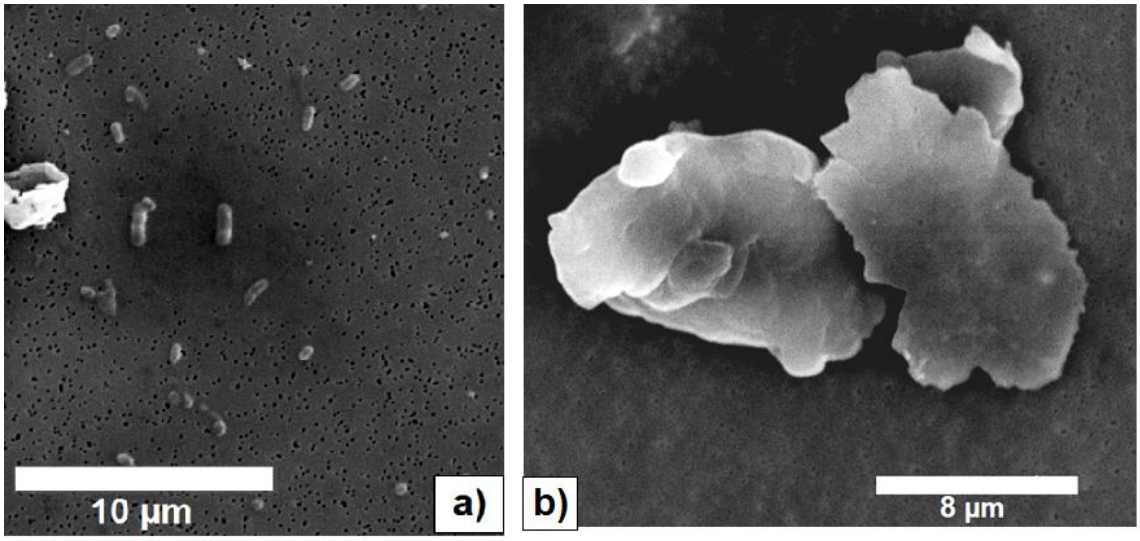

Figure 19: a) Small, round particles are presumed to originate from the plastic deformation layer, and are rounded as they tumble among ripples, while b) larger particle float above the ripples, and are flattened by the counterface into thin flakes.

3.4 Conclusions

- UHMWPE experiences multiple wear mechanisms, one of which is characterized by the accumulation of plastic deformation occurring in a thin surface layer. Evidence for such behavior was found in numerical simulations using actual surface geometries imported into Abaqus software. A novel testing method involving a small groove on the wear surface provided additional experimental evidence for this behavior.
- The grooved-surface testing also revealed that larger, flake-like particles cling to the polymer wear surface, and these particles can migrate across the surface. These

particles are similar in size and shape to the transfer film deposits made by certain polymers onto metal counterfaces, however, instead of being deposited onto the counterface, they remain adhered to the polymer bulk. The movement and deformation of these "self-adhering transfer films" may contribute to the low wear rate of UHMWPE.

- The presence of a thin, deformed layer at the polymer wear surface provides the first theoretical model for describing the unusual "rippled" geometry often found on UHMWPE components: The thin layer is plastically deformed by the sliding action of the counterface, but once released, it is compressed back towards its original shape by the bulk of the underlying polymer, leading to a buckling phenomenon with an equilibrium geometry described by a sinusoidal wave.
- The surface deformation layer in conjunction with the sinusoidal surface geometry creates independent regions of high stress and localized deformation, which are hypothesized to relate directly to the small, round wear particles seen in previous studies through a drawing action that occurs on the peaks of the sinusoidal surfaces.

3.5 References

[1] B.D. Garg, S.H. Cadle, P.A. Mulawa, P.J. Groblicki, C. Laroo, G.A. Parr, Brake Wear Particulate Matter Emissions, Environmental Science & Technology, 34 (2000) 4463-4469.

[2] W.F. Rogge, L.M. Hildemann, M.A. Mazurek, G.R. Cass, B.R.T. Simoneit, Sources of fine organic aerosol. 3. Road dust, tire debris, and organometallic brake lining dust: roads as sources and sinks, Environmental Science & Technology, 27 (1993) 1892-1904.

[3] V. Colvin, The potential environmental impact of engineered nanomaterials, Nature Biotechnology, Nature Publishing Group, 2003, pp. 1166.

[4] J.H. Dumbleton, M.T. Manley, A.A. Edidin, A literature review of the association between wear rate and osteolysis in total hip arthroplasty, The Journal of Arthroplasty, 17 (2002) 649-661.

[5] M. Endo, J.L. Tipper, D.C. Barton, M.H. Stone, E. Ingham, J. Fisher, Comparison of wear, wear debris and functional biological activity of moderately crosslinked and non-crosslinked polyethylenes in hip prostheses, Proceedings of the I MECH E Part H Journal of Engineering in Medicine, 216 (2002) 111-122.

[6] O. Muratoglu, D. O'Connor, C. Bragdon, E. Al., Gradient crosslinking of UHMWPE using irradiation in molten state for total joint arthroplasty, Biomaterials, 23 (2002) 717-724.

[7] E. Oral, K.K. Wannomae, N. Hawkins, W.H. Harris, O.K.O.K. Muratoglu, [alpha]-Tocopherol-doped irradiated UHMWPE for high fatigue resistance and low wear, Biomaterials, 25 (2004) 5515-5522.

[8] G. Guofang, G. Guofang, Y. Huayong, F. Xin, Tribological properties of kaolin filled UHMWPE composites in unlubricated sliding, Wear, 256 (2004) 88.

[9] M. Zhang, R. King, M. Hanes, S.P. James, A novel ultra high molecular weight polyethylene-hyaluronan microcomposite for use in total joint replacements. I. Synthesis and physical/chemical characterization, J Biomed Mater Res A, 78 (2006) 86-96.

[10] D.S. Xiong, J.M. Lin, D.L. Fan, Wear properties of nano-Al2O3/UHMWPE composites irradiated by gamma ray against a CoCrMo alloy, Biomedical Materials, 1 (2006) 175-179.

[11] K. Plumlee, C.J. Schwartz, Improved wear resistance of orthopaedic UHMWPE by reinforcement with zirconium particles, Wear, 267 (2009) 710-717.

[12] K. Plumlee, C. Schwartz, Investigating UHMWPE wear mechanisms by decomposing wear debris distributions, Wear, 271 (2011) 2208-2212.

[13] J. Dowling, J. Atkinson, D. Dowson, J. Charnley, THE CHARACTERISTICS OF ACETABULAR CUPS WORN IN THE HUMAN BODY, Journal of Bone and Joint Surgery, 60-B (1978).

[14] A. Wang, C. Stark, J.H. Dumbleton, Role of cyclic plastic deformation in the wear of UHMWPE acetabular cups, Journal of Biomedical Materials Research, 29 (1995) 619-626.

[15] N. Suhendra, G.W. Stachowiak, Computational model of asperity contact for the prediction of UHMWPE mechanical and wear behaviour in total hip joint replacements, Tribology Letters, 25 (2007) 9-22.

[16] C.M. Stafford, B.D. Vogt, C. Harrison, D. Julthongpiput, R. Huang, Elastic Moduli of Ultrathin Amorphous Polymer Films, Macromolecules, 39 (2006) 5095-5099.

[17] R. Huang, Z. Suo, Wrinkling of a compressed elastic film on a viscous layer, Journal of Applied Physics, 91 (2002) 1135-1142.

[18] B. Audoly, A. Boudaoud, Buckling of a stiff film bound to a compliant substrate—Part I:: Formulation, linear stability of cylindrical patterns, secondary bifurcations, Journal of the Mechanics and Physics of Solids, 56 (2008) 2401-2421.

[19] S. Bahadur, The development of transfer layers and their role in polymer tribology. Wear. 245 (2000) 92-99.

[20] H. McKellop, P. Campbell, et al., The Origin of Submicron Polyethylene Wear Debris in Total Hip-Arthroplastiy. CLINICAL ORTHOPAEDICS AND RELATED RESEARCH. 311 (1995) 3-20.

[21] T. Asano, M. Akagi, et al., Dose effects of cross-linking polyethylene for total knee arthroplasty on wear performance and mechanical properties. Journal of Biomedical Materials Research Part B: Applied Biomaterials. 83B (2007) 615-622

4. INVESTIGATON OF CHARACTERISTIC RIPPLING TOPOLOGY PRODUCED DURING UHMWPE SLIDING[3]

4.1 Introduction

Ultra-high molecular weight polyethylene (UHMWPE) remains the most popular bearing material for use in artificial joints. As a result, the wear of UHMWPE has been studied extensively, mostly focused on the negative effect of wear debris on the body [1], and various techniques to reduce the total wear volume, such as crosslinking [2-7], and composite fillers [8-14]. Despite the quantity of studies, very little is known about the actual wear mechanisms that contribute to the removal of debris from the bulk.

Looking for insight into wear mechanisms, observation of the resultant wear surface reveals a polymer surface generally free cracking and deep abrasive scratches, but does result in a surface showing a periodic, rippled geometry whose wavelength closely matches debris size, with evidence that debris is removed from the peaks of each ripple. This geometry has been observed in many studies on retrieved implants [15, 16] and wear simulators [13, 17-21], and dates back at least as far as 1978, when Dowling and Charnley stated "the cause of the parallel ripples has not yet been identified" [15]. Since then, multiple mechanisms have been proposed for the formation of these ripples, including abrasion [22], crystallinity effects [13, 19, 23], fatigue [24, 25], stick-slip behavior [18,

[3] Manuscript to be submitted for publication

26], thermal softening [27, 28], and Schallamach waves [29, 30]. While the root cause may not be known, it is generally accepted that most bioactive debris particles originate from the peaks of these ripples, and that plastic deformation of the surface plays a role. In 1995, Wang, Stark, and Dumbleton reached similar conclusions, stating "It is still not well understood how the ripples are formed...but it is generally accepted that accumulated plastic deformation plays a critical role in the formation of the ripple-like features on the surface of the acetabular cups [17]." Previous studies have shown experimental evidence of shear strain 5-10 μm below the surface [31], and shown that crystalline lamella within the polymer orient along the direction of plastic deformation up to a depth of at least 4-10 μm [32].

One possible explanation for the ripples sprouts from the idea that the aforementioned plastic deformation occurs at the surface without that material being detached from the bulk [31, 32], resulting in a strained surface layer that eventually buckles as the stress relaxes. If the strained surface layer is uniform in thickness, the buckling film would form a periodic pattern perpendicular to the principle stress direction [20, 33]. Similar results have been seen in thin-film depositions of polymers onto metals [34]. In this case, the wavelength of the ripples, λ, is determined by the coordinated buckling and stretching of the film and substrate, described in the following equation [33],

$$\lambda = 2\pi h_f \left(\frac{E_f/(1-\nu_f{}^2)}{3 \cdot E_s/(1-\nu_s{}^2)}\right)^{\frac{1}{3}} \qquad \text{(Eq. 1)}$$

Where E is Young's modulus, h is the thickness of the film, and ν is Poisson's ratio. Subscripts of *f* and *s* refer to the film layer and the substrate, respectively. Assuming this same mechanism applies to the case of UHWMPE wear, the properties of both the

film and substrate would derive from the polymer, and would be similar in value. Moreover, within the equation, these materials properties are under a cubic root, therefore, any differences that arise between the film and substrate have a small effect on the wavelength. The film thickness is far more influential on wavelength, and would presumably be determined by the penetration depth at which material experiences yield. This implies that wear parameters related to polymer yielding would also affect the ripple wavelength, thereby providing useful avenues for exploring the mechanism.

The current standard for predicting the onset of plastic deformation in polymers is the Von Mises yield criterion, also known as the J_2-plasticity theory. This theory is often applied to ductile materials, and is particularly common in computer modeling. Unfortunately, there is evidence that Von Mises stress is not ideal for use in UHMWPE wear [35]. Additionally, the size scale of wear phenomena (< 1 μm) are on the border of necessitating the inclusion of additional molecular factors, such as individual chain alignment, semicrystalline regions, and intermolecular forces; all of which may lead to anisotropy within the material. These effects are not typically included in Von Mises yield criterion or continuum mechanics (and subsequently, finite element analysis), and therefore may not accurately predict the formation of surface films or ripples.

This study aims to explore the connection between the traditional Von Mises method of predicting yield and the experimentally observed rippling in a polymer wear surface, both to provide a link between simple mechanics and wear mechanisms, and to expose where these models fall short.

4.2 Materials and Methods

4.2.1 Computational Modeling

Finite element analysis (FEA) was performed using a commercial software package (ANSYS 18.0 Structural Analysis). Surface profile data was collected from worn samples via atomic force microscopy (Asylum MFP-3D), and non-contact, white light profilometry (Zygo). This data was imported into the finite element model as four-noded, 2-D plane strain elements, and was selected to ensure that both bodies had multiple asperities represented. Stress-strain behavior for GUR-4150 was taken from published data from ISO-527 tensile tests [36], and was imported as a multi-linear kinematic hardening curve, shown in Figure 20. The bulk physical properties applied for stainless steel and UHMWPE are seen in Table 1. A friction coefficient of 0.1 was applied within the software.

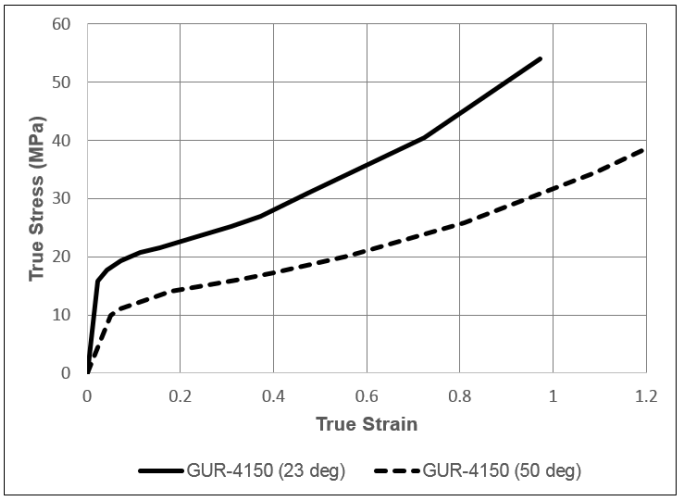

Figure 20: UHWMPE properties used in FEA, at 28° C (solid), and 50° C (dashed).

Table 1: Physical properties of materials used in FEA.

	Density (kg/m^3)	Modulus (GPa)	Poisson's Ratio
Stainless Steel	7750	193	0.31
GUR-4150 (23° C)	930	0.68	0.4
GUR-4150 (50° C)	930	0.2	0.4

For boundary conditions, the base of the UHMWPE body was fixed, and mirror boundaries were applied to the sides. The comparatively short counterface body was positioned above the UHWMPE body to ensure the part would remaining fully supported, then a pressure (2 or 6 MPa) was applied to the back counterface, forcing the two components together, as shown in Figure 21. Load levels were chosen to fall within the range of expected loads for artificial hips of less than 10 MPa [37], while allowing for ease of experimental testing later in the study. Once the bodies had come into contact, the counterface was displaced a distance of 5 μm while still under load. Meshing was refined using an automatic convergence tool within ANSYS, which refined the mesh near high stress areas until the regions changed by less than 3% with each subsequent step (Fig. 22). The final mesh had elements near the surface that were relatively equiaxed, approximately 75nm across, but elements got larger as they were further from the contact points. Maximum Von Mises stress and maximum plastic strain levels were recorded. To estimate the thickness of the deformed layer thickness for use in Equation 1, the maximum perpendicular distance from the contact surface to a sub-surface location where the plastic deformation exceeded 0.001 strain was recorded.

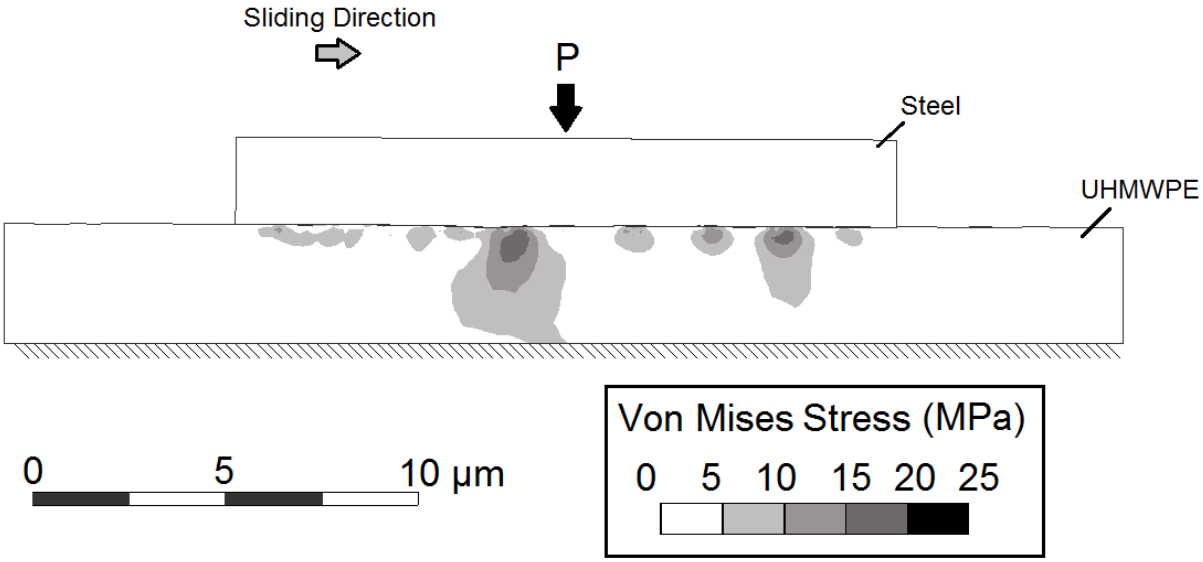

Figure 21: Example finite element model using imported surface geometries and contact pressure, P, of 6 MPa. Von Mises stresses are shown for UHWMPE body, on lower portion.

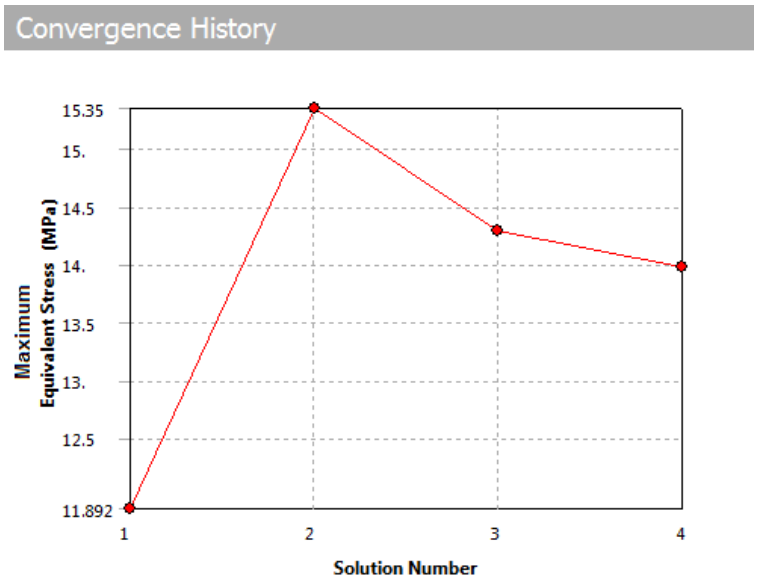

	Equivalent Stress 2 (MPa)	Change (%)	Nodes	Elements
1	11.892		2308	698
2	15.35	25.388	3022	926
3	14.295	-7.1222	4530	1416
4	13.982	-2.2132	5367	1689

Figure 22: Convergence plot of FEA mesh.

Experimental Tests:

Experimental wear tests were performed to explore the range and consistency of the wear behavior at the same conditions as investigated during the computer simulations. These tests were performed using GUR-4150 (Ticona), which was compression molded into cylinders, 6.25 mm in diameter and cut 18 mm in length. Tests were conducted on a custom built wear testing device (Fig. 23), which provides two axes of motion, and uses variable pneumatic cylinders to apply contact pressure between the samples and the counterfaces. Counterfaces consisted of 90mm square plates made from stainless steel (type 410, 45 HRC), which were polished to two different degrees of roughness values:

R_a = 0.005 μm and 0.030 μm). The polymer specimens traced out 50 mm diameter circles at a speed of 70 rpm for 72 hours (approximately 250,000 cycles).

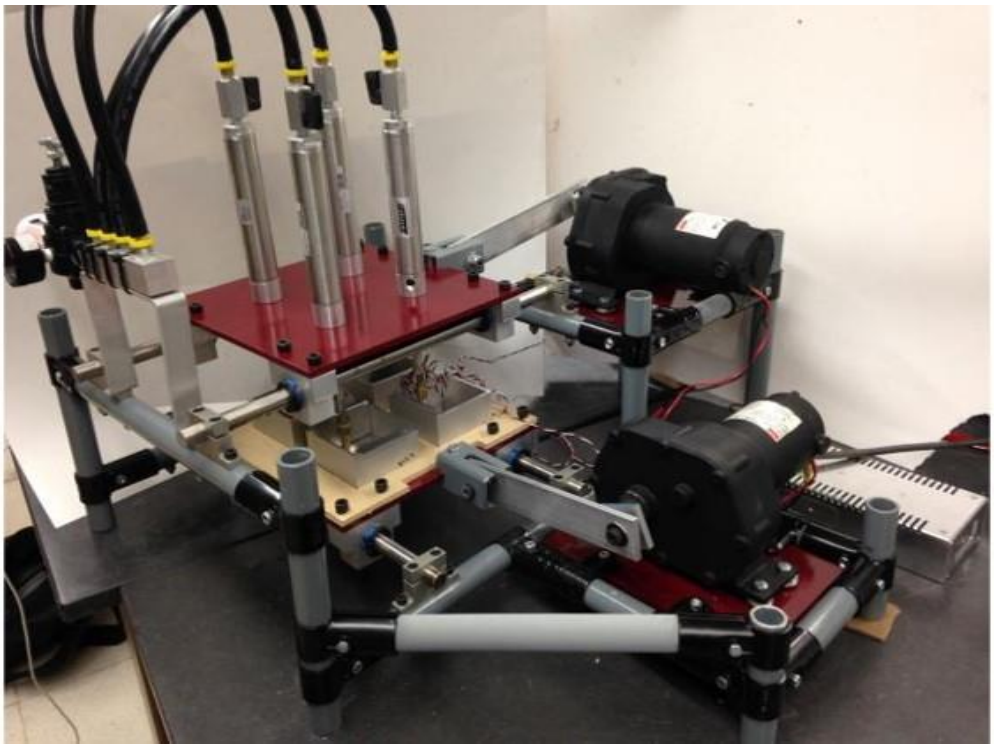

Figure 23: Custom Built, two-axis wear machine. Up to four UHMWPE cylinders affix to individual pneumatic cylinders, which are attached to the upper plate. This plate slides back and forth, linearly, via an electric gear motor and crank. The lower plate holds corresponding individual counterfaces, and is driven in a perpendicular direction, resulting in a circular wear path between counterface and UHWMPE pins. An electric heater is applied to the bottom of the lower plate to control the temperature of the counterfaces.

Experimental wear tests were performed at contact pressures of 2 MPa and 6 MPa, to match the numerical models discussed previously, and to balance the size and torque constraints of the test apparatus. The temperature of the counterface was regulated to either 28° C or 50° C (± 1° C) through a heat strip applied to the back of the counterface, and controlled via temperature controller and thermocouple, and verified with an infrared

thermometer. Each test setting was repeated twice to confirm the consistency and repeatability of each test setting.

Previous studies of UHWMPE wear surfaces have revealed widespread periodic geometries, often referred to as ripples or wrinkles. They typically range from 0.5 to 5 μm in wavelength, with total heights less than 1 μm. The general shape is loosely sinusoidal, although the peaks are often flattened or drawn out into fingers, suggesting that small debris particles are liberated from these asperities.

At the conclusion of each wear test, the resultant wear surface was imaged using a Zeiss NEON scanning electron microscope, with specific focus on ripple geometries. Ripple wavelength from these images was measured using ImageJ software. To get a thorough sampling of wavelength, measurements were taken by averaging the length across multiple ripple peaks, and this process was performed multiple times across each SEM image. Each sample was imaged multiple times across the surface, and each image covered a width of approximately 30-50 wavelengths to maintain adequate resolution.

By comparing the predicted effects of wear conditions from models to the experimentally observed ripple wavelength, it is possible to make indirect conclusions about of the existence of a thin film of plastically deformed material and its role in ripple development. For additional observation and support of these claims, a novel method was employed to experimentally observe the thickness of the deformation layer, which also allowed for observing geometry changes over a few cycles, rather than just a single snapshot. To accomplish this, additional wear samples were generated by wearing specimens according to the same test parameters as above, then “notching” the wear

surface by lightly scratching across the center with a fresh razor blade. This gouge left a clean groove in the wear surface, approximately 10 μm across. Grooved samples were then placed back in the wear test machine and worn for a small number of additional cycles and SEM images were collected. Any plastic deformation that occurs at the surface would modify the geometry of the groove, providing insight into the distribution of plastic deformation and the thickness of the layer.

4.3 Results and Discussion

4.3.1 Finite Element Results

Finite element models revealed that all test settings experienced plastic deformation at the surface of the polymer, but the extent of plastic deformation varied in both penetration depth and magnitude, as summarized in Table 2. In all of the simulations, regions of high stress were limited to the asperities, with regions of virtually zero stress in the valleys. In spite of the early expectations that counterface roughness would play a key role in the depth that plastic deformation occurred, it was observed that it had little effect. This is likely due to the fact that the imported geometry of the worn polymer surface had a roughness comparable to the rough counterface (R_a = 0.03 μm), so that the locations that experienced the highest stresses in any given simulation were mostly dependent on polymer asperities, rather than counterface roughness. Choosing a counterface significantly rougher than the polymer surface could result in more pronounced effects, causing more localized stresses and thicker deformation layers.

Similarly, the combined effects of temperature on both yield and modulus appeared to balance out, resulting in a very little effect on the magnitude or depth of plastic deformation within the simulations. While it is well known that both temperature and roughness can affect the wear rate and mechanisms [38, 39], the range of values used within this study were deliberately chosen so that all samples would maintain similar mechanisms for ripple formation. The lack of strong correlations between these factors suggests that slight variations in these parameters makes little difference in plastic deformation at the surface, and therefore little change to ripple wavelength. This is supported by the consistency in ripple wavelength seen across literature.

Table 2: Data from FEA results for Plastic Deformation. Maximum Von Mises strain and maximum thickness of deformed layer.

Maximum strain at various test settings.

	Low Roughness		**High Roughness**	
	Low Temp	**High Temp**	**Low Temp**	**High Temp**
Low Pressure	0.0476	0.0153	0.0211	0.0247
High Pressure	0.0765	0.0879	0.0905	0.0685

Thickness of Deformed layer (μm) at various test settings

	Low Roughness		**High Roughness**	
	Low Temp	**High Temp**	**Low Temp**	**High Temp**
Low Pressure	1.08	0.48	0.53	0.54
High Pressure	1.55	1.02	1.59	1.25

The most notable influence seen in the simulations was that of contact pressure on the thickness of the layer of plastically deformed material (3-factor ANOVA, $p = 0.09$). At the lowest contact pressures (2 MPa applied pressure), the strained polymer results in an inconsistent layer of plastically deformed material, with a penetration depth less than 0.5 μm. In contrast, higher contact pressures (6 MPa applied pressure) produced plastic deformation in a layer almost 1 μm thick, which grew laterally across the surface as the counterface asperity moved, creating a more continuous surface layer of deformation. The deformed region extended approximately twice as deep into the polymer bulk as compared to the lower pressure. This would suggest that increasing pressure would increase the thickness of the strained surface layer, thereby increasing ripple wavelength, according to thin-film theory shown in Eq. 1.

Most notably, finite element models did not demonstrate continued accumulation of strain over repeated cycles, nor did they show failure of material, despite experimental evidence that the peaks of rippled formations are drawn out until failure [17]. Instead, simulations showed that as asperities slid across each other, strain hardening of the polymer resulted in a plateau of accumulated strain, typically after only one or two passes (Fig. 24). The strain that did occur was in a smooth gradient throughout the depth of the affected region.

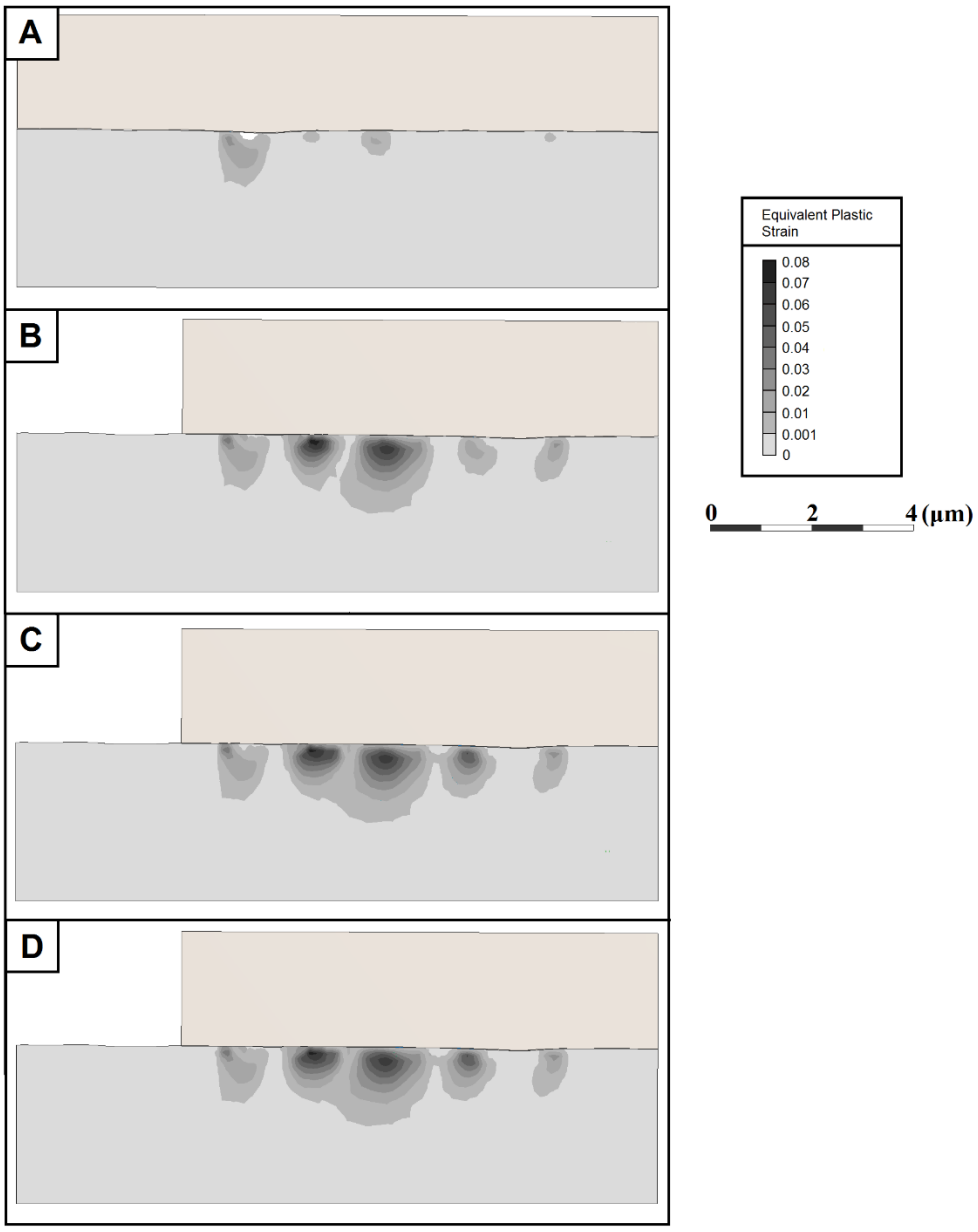

Figure 24: Finite element results for accumulated plastic deformation between imported surface profiles for worn UHMWPE and smooth (R_a = 0.005 µm) stainless steel counterface at 6MPa contact pressure. (A) At initial loading, (B) after 1 pass, (C) after 3 passes, and (D) after 7 passes. Almost no additional strain accumulates after first three passes.

4.3.2 Experimental Results

Ripples were observed in all test specimens to varying degrees, and wavelengths were recorded from multiple locations across a sample face, with a minimum of ten measurements for each sample. The ripple formations could be easily classified into two main types based on extent of coverage: fully-developed, which covered large areas, and under-developed, which covered much smaller areas. These two groups were also easily distinguished by wavelength, as seen in Figure 25.

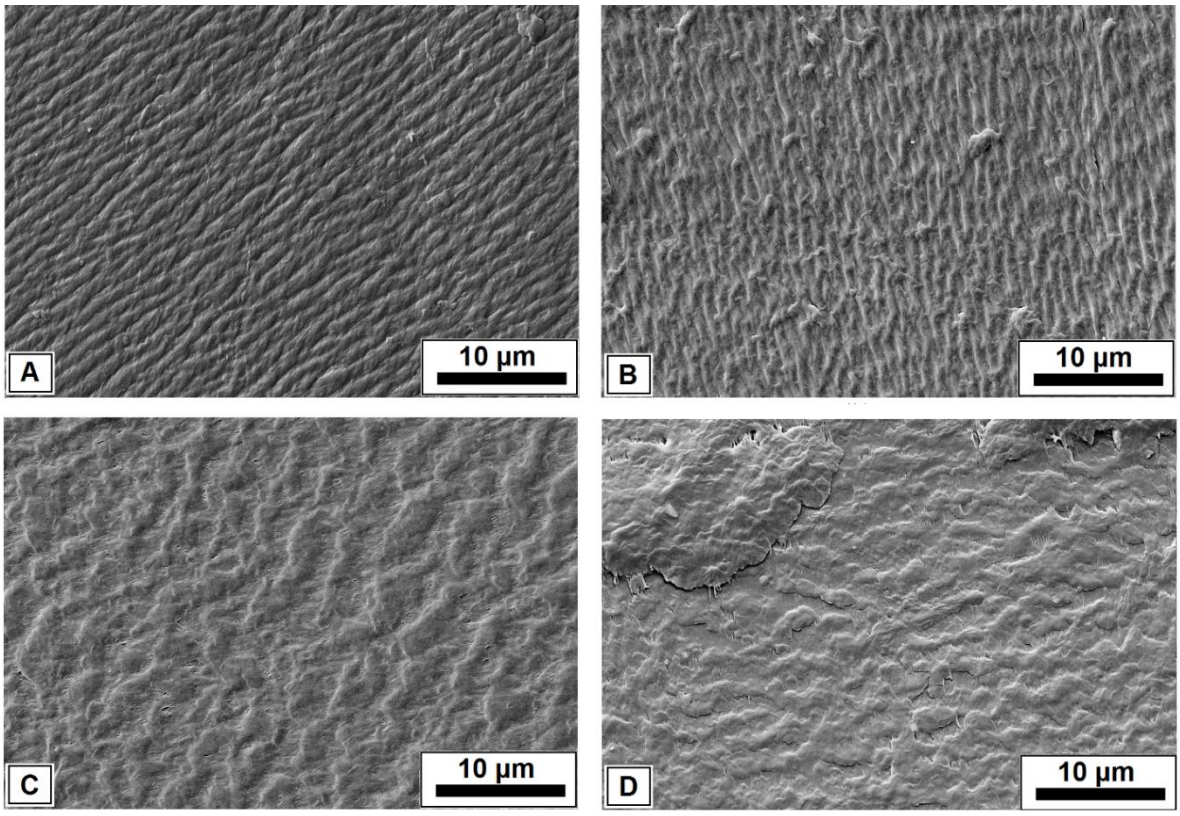

Figure 25: Fully developed rippled regions from UHWMPE worn against smooth stainless steel at 28° C, at (A) 2 MPa pressure, and (B) 6 MPa pressure. Underdeveloped rippled regions in samples worn against smooth stainless steel and 2 MPa pressure, but at 50° C (C and D).

The variation between samples suggests that the formation of ripples was more dynamic than initially predicted. Two possible explanations are presented here: 1) the rippled surface feature is indeed a steady-state phenomena, but the difference in test settings require different durations to achieve steady state, and therefore produced different levels of development, or 2) the ripples are not a steady feature, but instead progress through a cycle of development, wearing down, and regeneration as material is removed from the bulk.

A 3-way ANOVA study revealed the distinction between fully developed and under developed ripples was closely correlated to the interaction between temperature and pressure ($p = 0.08$), although the limited number of samples used in this exploratory study limit the power of the test. It has been previously shown that the coefficient of friction changes with temperature, as does wear rate [38], which could explain the interaction, although more in-depth analysis is needed. Although certain test parameters consistently resulted in fully developed ripples, most settings resulted in a combination of both types of ripples, suggesting that ripple formation is a dynamic process. A summary of the results can be seen in Figure 26.

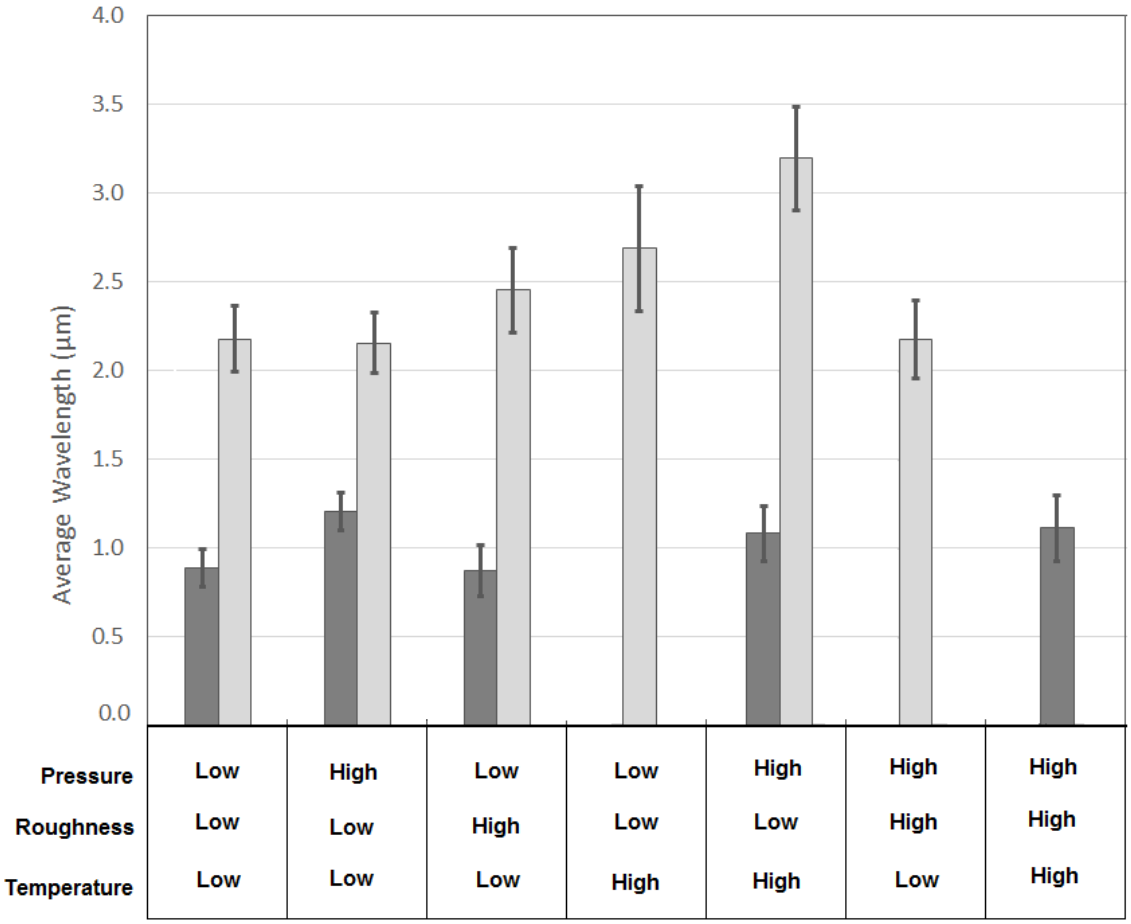

Figure 26: Overview of ripple wavelength across multiple samples based on test setting, with error bars showing one standard deviation. Ripples were categorized into two distinct groups: fully developed ripples (dark grey) covered regions hundreds of wavelengths wide, while underdeveloped ripples (light grey) were less consistent and covered small areas.

It is hypothesized that these two different groups are due to differences in the evolution of the wear surface. To maintain consistency in this study, every sample was worn for the same duration of time; however, not every sample had the same mass loss rate. It is expected that the fully developed ripples were more representative of samples that achieved near steady state conditions, and are therefore better matches for finite

element models. Underdeveloped samples have less consistent surfaces, and are likely the result of not yet achieving steady conditions. For the sake of simplifying analysis, these two groups were treated separately.

Fully developed ripples were found in nearly every combination of test parameters, and remained consistent from sample to sample, with the average wavelength ranging from 0.8 to 1.2 μm across all samples. These regions covered significant portions of the wear surface, extending many hundreds of micrometers across or more, even up to the edge of the sample, as seen in Figure 27. Despite the similarity between all these samples, one-way ANOVA analysis suggests that these are independent, and do not have the same average wavelength ($p < 0.001$). However, three-factor analysis did not reveal any significant correlations between wavelength and any test parameters (pressure, temperature, or roughness). This is in opposition to the finite element results, which suggested pressure should be a strong correlation. It is noted that pressure was in fact the strongest relation at a p-value of 0.21, and the limited number of samples and the previously mentioned changes in coefficient of friction and wear rate might be blurring some of the effects.

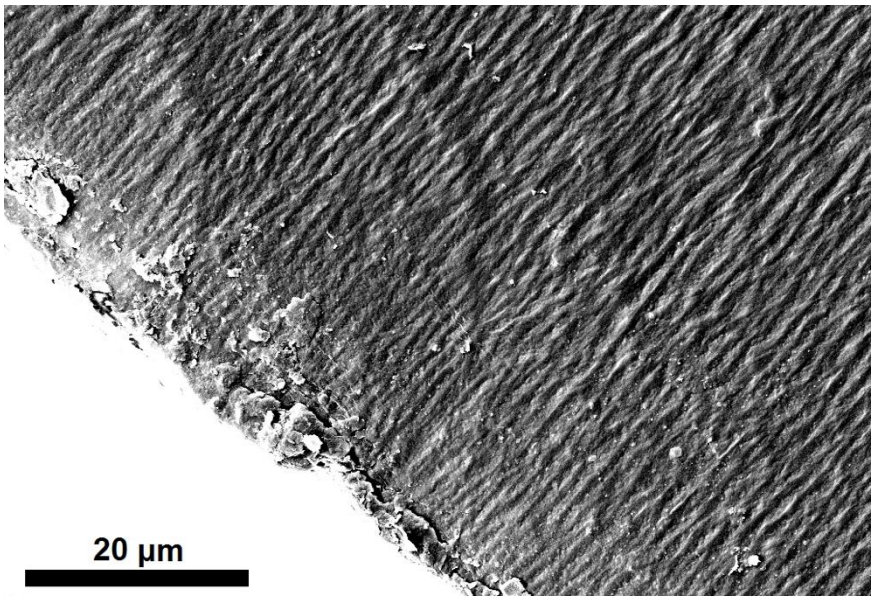

Figure 27: Ripples extend almost completely to edge of sample, without noticeable change in wavelength.

Additional observations from the fully developed regions include changes in directionality of the ripples. On a local scale of a few hundred microns, the ripples appear to maintain a relatively uniform direction and consistent spacing, but across the full span of the sample, the direction of the ripples changes (Fig. 28) and the wavelength may vary by up to 40%. The change in direction can be explained by a preferential stress direction that arises due to the flexure of the sample. As the sample moves in a circular pattern, the sample bends slightly due to friction, creating an uneven load profile across the surface. This has two implications: 1) the samples are not experiencing symmetric, two-axis motion, implying that chain orientation is likely present, and 2) the average contact pressures experienced by the sample may be significantly greater than the expected values. This behavior was not captured in 2D finite element models.

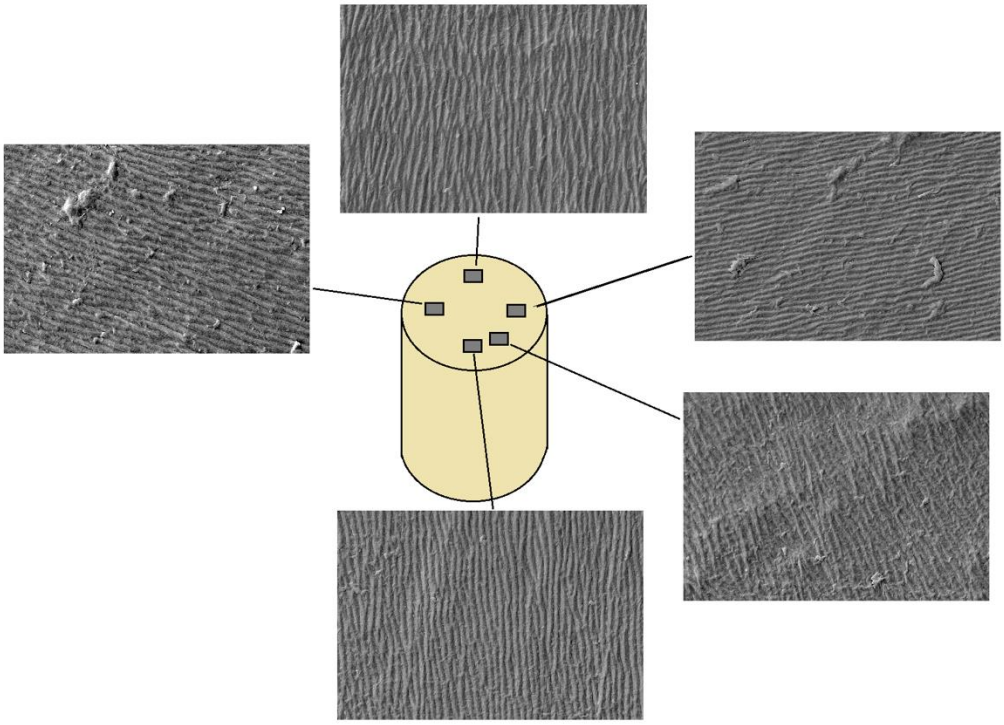

Figure 28: The orientation of the ripples varied depending on the location around the perimeter of the wear surface, due to the flexure of the sample under frictional load, resulting in a preferential stress direction. All images were taken from the same sample, and are shown in same scale. The ripple wavelength varies by up to 40% from image to image.

Alternatively, the under-developed ripples had much smaller regions of coverage, and the individual patterns were far less defined and consistent. Additionally, the wavelength was between two and three times as large as the fully developed ripples, ranging from 2.15-3.15 μm in wavelength. Analysis of the results suggests the spacing associated with this phenomenon has a reasonably strong dependence on temperature. It is suspected this phenomenon is associated wear processes that are approaching, but have not quite achieved, steady state conditions. At these premature times, contact stresses

would be less uniform, and layers of deformed material would be present but less consistent, resulting in loose semi-rippled geometry. As the samples continues to wear, the strained layer becomes more widespread, thinner, and crisper in detail, giving smaller ripples. Supporting this hypothesis, Barrett *et al* demonstrated that both the wear rate and friction coefficient of UHWMPE on stainless steel are dynamic, particularly between 50° C and 66° C [38], noting that larger debris flakes form in higher temperatures, which disrupt the wear surface. This dynamism would result in poor film generation, and would explain the relationship between wavelength and temperature – cooler temperatures experience more steady wear, and therefore more consistent ripples. It is possible that the conditions would eventually stabilize, in which case, ripple wavelength would only be dependent on temperature early in the wear process, but would become less influenced by temperature as steady state conditions are reached. This would match the results of computer models, since the simulations were performed using steady state surface geometries and conditions. Longer wear tests would need to be performed to verify this hypothesis.

4.3.3 Grooved-Surface Testing Results:

With limited correlation between computational simulations based on Von Mises stress and experimental results, focus was shifted towards additional methods for exploring and confirming the level of plastic deformation at the surface, which was accomplished through the use of the grooved-surface testing. Freshly grooved samples that experienced no additional wear were observed to have clean groove edges in SEM

images, whereas grooved sample that had additional wear cycles experienced noticeable changes to the groove geometry (Fig. 29). These changes occurred in as little as a single cycle, and are observed across the entire surface of the sample, suggesting that large-scale plastic deformations does indeed occur, although in greater magnitudes than predicted by finite element models. Occasional flake-like debris, typically associated with adhesive wear, were also seen bridging the groove, acting as a self-adhering transfer film which remains relatively mobile as these particles migrate across the wear surface.

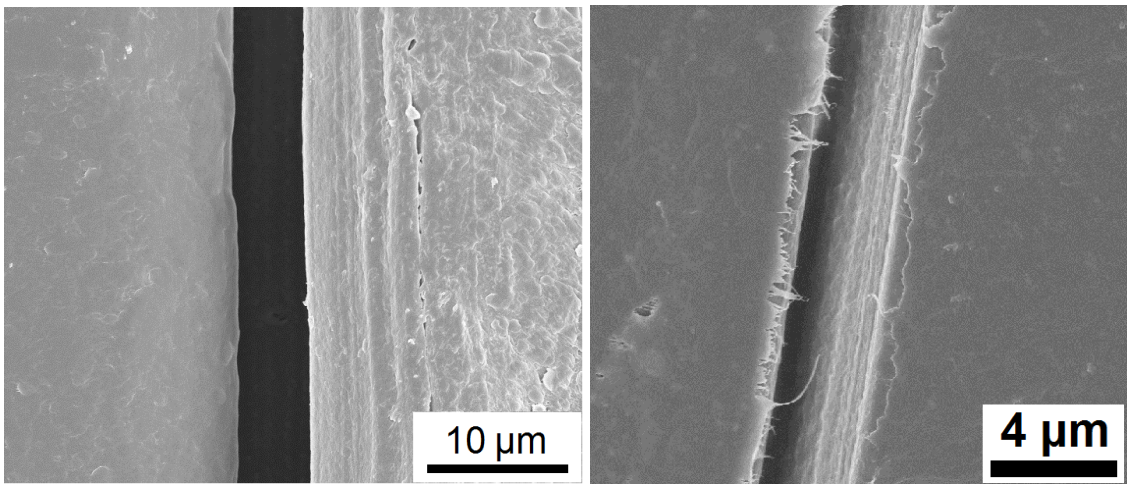

Figure 29: Pristine notch with no additional wear cycles (left). Notch after 3 cycles of motion at 2 MPa and smoothest counterface (right). Finite element models based on Von Mises stress for these conditions predict yield to occur at depths of 1 µm from surface, which is not observed.

The typical formations seen near the notch boundary include thin sheets and fingers that appear to be much less than 1 µm in thickness, significantly thinner than any Von Mises stress models suggested. Additionally, the finite element models suggested a smooth gradient of deformation penetrating into the bulk surface layer up to 1 µm, whereas

the notch test results show the thin film is reasonably discontinuous from the bulk surface (Fig. 30). These thin sheet formations occurred in every sample setting, and no difference in film thickness or coverage was noted between settings was noted, based purely on visual inspection. Better measurements may reveal more insight into these deformation mechanisms, however, when higher magnification images were attempted in the SEM, the extremely thin polymer sections experienced melting and warping.

The high level of deformation sustained by this layer in a single motion suggests this film behaves like a transfer film, allowing low friction and relative motion between the bulk polymer and the substrate. It is hypothesized that this transfer layer is created from a buildup of polymer that has already been liberated from the bulk. Since this layer is not affixed to the bulk, it would not be subject to Von Mises yield criteriam and would explain the lack of correlation to finite element models. Additionally, the influence of temperature on coefficient of friction and adhesion levels would also play a strong role in the development of ripples, as seen in the experimental results. Compared to the original hypothesis that the surface of the polymer bulk is experience plastic deformation, the mechanisms of ripple formation remain the same: relaxation of a strained polymer film; only now the mechanism of film generation is different.

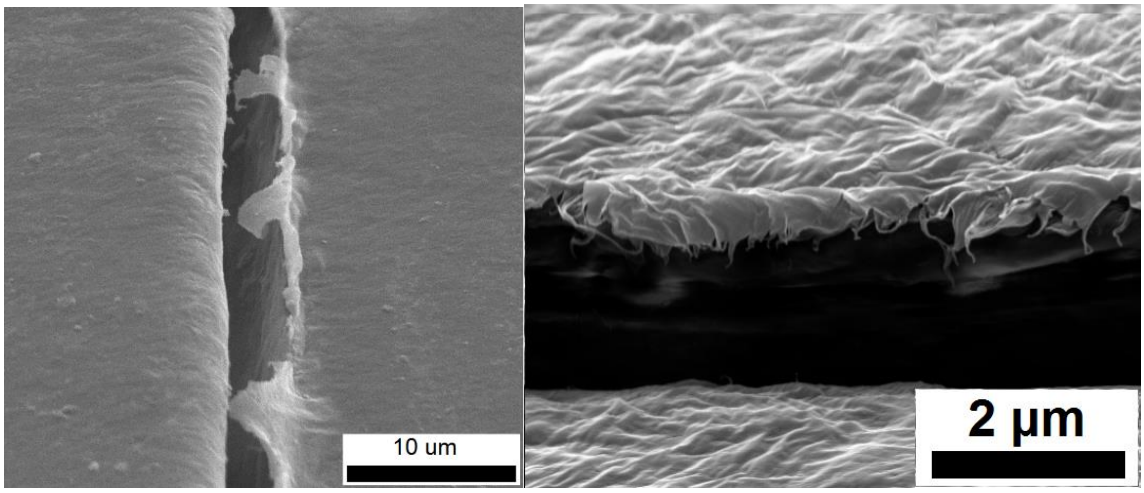

Figure 30: Worn notches viewed from 60° angle. In contrast to finite element models, there is no sign of a gradient of deformation penetrating up to 1µm into the surface, rather, a thin surface layer with drawn fingers, approximately 10-20nm in thickness is observed.

4.4 Conclusions

- Rippled surface geometries with wavelengths less of 5µm or less were observed in all samples, and were separated into two categories: widespread, continuous ripples that extended for hundreds of wavelengths; and discontinuous ripples that only extended for a small number of wavelengths. Discontinuous ripples had wavelengths approximately twice that of the continuous regions.
- Finite element analysis on imported surface geometries predicted plastic deformation for all test parameters according to Von Mises yield criterion, with contact pressure showing the most significant effect on the thickness of the deformed layer. In spite of these findings, experimental results did not show any relationship between contact pressure and observed ripple wavelength, or contact pressure and the thickness of observed deformation near notched geometries.

- Based on Von Mises stresses, finite element models suggest that layers up 1μm thick will experience plastic deformation over a smooth gradient. Observations of grooved samples show layers much thinner (on the order of 20nm), with little to no gradient of deformation into the material.
- Finite element results showed a plateau in the accumulation of strain due to strain-hardening effects, rather than a continual build up until failure. Experimental results show accumulation of plastic deformation, but no evidence of such a plateau. This, in combination with the small thickness and high level of deformation, suggests that future FEA work should consider use of more robust material models for UHWMPE, most likely including anisotropic properties, and the effects of adhesion with the counterface.
- Due to the thin cross-section and high mobility of the observed polymer film, it is hypothesized that the strained surface layer is acting as a self—adhering transfer film, made up of thin layers of debris already liberated from the bulk. This would match the lack of correlation between ripples and Von Mises yield criteria, but a strong correlation to temperature, which affects the development of ripples by affecting both the coefficient of friction and adhesion level between the film, the counterface, and the polymer bulk.
- The dynamic nature of surface development and the natural variations between samples requires a sufficient number of samples to ensure that results have the statistical power to detect differences in behavior.

4.5 References:

[1] J.H. Dumbleton, M.T. Manley, A.A. Edidin, A literature review of the association between wear rate and osteolysis in total hip arthroplasty, The Journal of Arthroplasty, 17 (2002) 649-661.

[2] E. Oral, S.D. Christensen, A.S. Malhi, K.K. Wannomae, O.K. Muratoglu, Wear Resistance and Mechanical Properties of Highly Cross-linked, Ultrahigh-Molecular Weight Polyethylene Doped With Vitamin E, The Journal of Arthroplasty, 21 (2006) 580-591.

[3] O.K. Muratoglu, C.R. Bragdon, D.O. O'Connor, M. Jasty, W.H. Harris, A novel method of cross-linking ultra-high-molecular-weight polyethylene to improve wear, reduce oxidation, and retain mechanical properties: Recipient of the 1999 HAP Paul Award, The Journal of Arthroplasty, 16 (2001) 149-160.

[4] G. Lewis, Properties of crosslinked ultra high molecular weight polyethylene, Biomaterials, 22 (2001) 371-401.

[5] M. Jasty, H.E. Rubash, O. Muratoglu, Highly cross-linked polyethylene: the debate is over--in the affirmative, J Arthroplasty, 20 (2005) 55-58.

[6] R. Chiesa, M.C. Tanzi, Alfonsi, Paracchini, Moscatelli, Cigada, Enhanced wear performance of highly crosslinked UHMWPE for artificial joints, Journal of Biomedical Res., 50 (2000) 381-387.

[7] J.A. Savio, L.M. Overcamp, J. Black, Size and shape of biomaterial wear debris, Clinical Materials, 15 (1994) 101-147.

[8] Q. Wang, J. Liu, S. Ge, Study on Biotribological Behavior of the Combined Joint of CoCrMo and UHMWPE/BHA Composite in a Hip Joint Simulator, Journal of Bionic Engineering, 6 (2009) 378-386.

[9] L. Fang, Y. Leng, P. Gao, Processing of hydroxyapatite reinforced ultrahigh molecular weight polyethylene for biomedical applications, Biomaterials, 26 (2005) 3471-3478.

[10] C.H. Navarro, K.J. Moreno, A. Chávez-Valdez, F. Louvier-Hernández, J.S. García-Miranda, R. Lesso, A. Arizmendi-Morquecho, Friction and wear properties of poly(methyl methacrylate)–hydroxyapatite hybrid coating on UHMWPE substrates, Wear, 282-283 (2012) 76-80.

[11] S. Ge, S. Wang, X. Huang, Increasing the wear resistance of UHMWPE acetabular cups by adding natural biocompatible particles, Wear, 267 (2009) 770-776.

[12] J. Tong, Y. Ma, M. Jiang, Effects of the wollastonite fiber modification on the sliding wear behavior of the UHMWPE composites, Wear, 255 (2003) 734-741.

[13] C.J. Schwartz, S. Bahadur, S.K. Mallapragada, Effect of crosslinking and Pt–Zr quasicrystal fillers on the mechanical properties and wear resistance of UHMWPE for use in artificial joints, Wear, 263 (2007) 1072-1080.

[14] Y. Chen, Y. Qi, Z. Tai, X. Yan, F. Zhu, Q. Xue, Preparation, mechanical properties and biocompatibility of graphene oxide/ultrahigh molecular weight polyethylene composites, European Polymer Journal, 48 (2012) 1026-1033.

[15] J.M. Dowling, D. Dowson, J. Charnley, The characteristics of acetabular cups worn in the human body, Bone & Joint Journal, 60 (1978) 375-382.

[16] A. Wang, C. Stark, J.H. Dumbleton, Mechanistic and Morphological Origins of Ultra-High Molecular Weight Polyethylene Wear Debris in Total Joint Replacement Prostheses, Proceedings of the Institution of Mechanical Engineers, Part H: Journal of Engineering in Medicine, 210 (1996) 141-155.

[17] A. Wang, C. Stark, J.H. Dumbleton, Role of cyclic plastic deformation in the wear of UHMWPE acetabular cups, Journal of Biomedical Materials Research Part A, 29 (1995) 619-626.

[18] J. Wang, F. Yan, Q. Xue, Friction and Wear Behavior of Ultra-High Molecular Weight Polyethylene Sliding Against GCr15 Steel and Electroless Ni–P Alloy Coating Under the Lubrication of Seawater, Tribology Letters, 35 (2009) 85-95.

[19] J. Zhou, K. Komvopoulos, Wear mechanisms of untreated and gamma irradiated ultra-high molecular weight polyethylene for total joint replacements, ASME/STLE 2004 International Joint Tribology Conference, American Society of Mechanical Engineers, 2004, pp. 1767-1773.

[20] K.G. Plumlee, C.J. Schwartz, Surface layer plastic deformation as a mechanism for UHMWPE wear, and its role in debris size, Wear, 301 (2013) 257-263.

[21] T. Asano, M. Akagi, I.C. Clarke, S. Masuda, T. Ishii, T. Nakamura, Dose effects of cross-linking polyethylene for total knee arthroplasty on wear performance and mechanical properties, Journal of Biomedical Materials Research Part B: Applied Biomaterials, 83 (2007) 615-622.

[22] C.H. da Silva, A. Sinatora, Development of severity parameter for wear study of thermoplastics, Wear, 263 (2007) 957-964.

[23] J. Tamura, I.C. Clarke, K. Kawanabe, M. Akagi, V.D. Good, P.A. Williams, T. Masaoka, D. Schroeder, H. Oonishi, Micro-wear patterns on UHMWPE tibial inserts in total knee joint simulation, Journal of Biomedical Materials Research Part A, 61 (2002) 218-225.

[24] C. McNie, D. Barton, E. Ingham, J. Tipper, J. Fisher, M. Stone, The prediction of polyethylene wear rate and debris morphology produced by microscopic asperities on femoral heads, Journal of Materials Science: Materials in Medicine, 11 (2000) 163-174.

[25] W. Shi, H. Dong, T. Bell, Tribological behaviour and microscopic wear mechanisms of UHMWPE sliding against thermal oxidation-treated Ti6Al4V, Materials Science and Engineering: A, 291 (2000) 27-36.

[26] J.H. Dieterich, Time-dependent friction and the mechanics of stick-slip, pure and applied geophysics, 116 (1978) 790-806.

[27] H. Unal, A. Mimaroglu, Friction and wear behaviour of unfilled engineering thermoplastics, Materials & Design, 24 (2003) 183-187.

[28] H.-C. Kuo, M.-C. Jeng, Dry Sliding Wear Properties of Ultra-high Molecular Weight Polyethylene Parts Made by the Injection Molding Process, Polymer-Plastics Technology and Engineering, 50 (2011) 604-612.

[29] A. Schallamach, How does rubber slide?, Wear, 17 (1971) 301-312.

[30] Q. Wang, Y. Wang, H. Wang, N. Fan, F. Yan, Experimental investigation on tribological behavior of several polymer materials under reciprocating sliding and fretting wear conditions, Tribology International, 104 (2016) 73-82.

[31] J.R. Cooper, D. Dowson, J. Fisher, Macroscopic and microscopic wear mechanisms in ultra-high molecular weight polyethylene, Wear, 162-164 (1993) 378-384.

[32] A.A. Edidin, L. Pruitt, C.W. Jewett, D.J. Crane, D. Roberts, S.M. Kurtz, Plasticity-induced damage layer is a precursor to wear in radiation-cross-linked UHMWPE acetabular components for total hip replacement, The Journal of Arthroplasty, 14 (1999) 616-627.

[33] C.M. Stafford, C. Harrison, K.L. Beers, A. Karim, E.J. Amis, M.R. VanLandingham, H.-C. Kim, W. Volksen, R.D. Miller, E.E. Simonyi, A buckling-based metrology for measuring the elastic moduli of polymeric thin films, Nature Materials, 3 (2004) 545.

[34] C.M. Stafford, B.D. Vogt, C. Harrison, D. Julthongpiput, R. Huang, Elastic Moduli of Ultrathin Amorphous Polymer Films, Macromolecules, 39 (2006) 5095-5099.

[35] J.S. Bergström, C.M. Rimnac, S.M. Kurtz, Prediction of multiaxial mechanical behavior for conventional and highly crosslinked UHMWPE using a hybrid constitutive model, Biomaterials, 24 (2003) 1365-1380.

[36] Ticona, GUR UHMWPE Product Brochure, Ticona GmbH, 2001.

[37] A. Wang, D. Sun, C. Stark, J. Dumbleton, Wear mechanisms of UHMWPE in total joint replacements, Wear, 181 (1995) 241-249.

[38] T.S. Barrett, G.W. Stachowiak, A.W. Batchelor, Effect of roughness and sliding speed on the wear and friction of ultra-high molecular weight polyethylene, Wear, 153 (1992) 331-350.

[39] B. Weightman, D. Light, The effect of the surface finish of alumina and stainless steel on the wear rate of UHMW polyethylene, Biomaterials, 7 (1986) 20-24.

5. GENERAL CONCLUSIONS

Despite its popularity in bearing applications, the complex wear behavior of UHWMPE against smooth metal counterfaces, as well as the mechanisms of debris production, continue to be challenging research questions. The work described herein has made progress in developing tools and techniques to better understand wear mechanisms and behaviors in UHMWPE. The following conclusions have been drawn from the results of this investigation:

1) The custom built, two-axis wear simulator used in this study was able to recreate wear debris and wear surfaces similar to those resulting from other accelerated wear test apparatus and from orthopedic implants.
2) In these biologically relevant conditions, UHWMPE appeared to wear according to multiple mechanisms. Debris analysis of size, shape, and complexity revealed a relatively small concentration of particles consistent with classic fatigue and abrasion processes, but a higher concentration of particles consistent with adhesive wear and transfer film development.
3) A high percentage of debris particles consisted of small, smooth, and rounded particles that do not correspond to any classic wear models. They have a similar size range to a surface rippling phenomenon, and it is hypothesized that both the ripples and the debris are the result of plastic deformation at the surface.
4) UHWMPE was confirmed to experience high levels of plastic deformation at the wear surface, even when subjected to nominal contact pressures well below the

yield stress. This was shown both in computer simulations and experimental results.

5) A novel notched surface approach was developed for observing surface deformation over incremental wear cycles. This approach revealed extremely thin sheets of deformation, down to 20 μm in thickness, which covered large expanses of the wear surface. This deformation mode was inconsistent with traditional finite element models, which predicted thicker deformation zones based on Von Mises yield criteria.
6) It is hypothesized that the thin surface layer of deformation will relax and buckle, and the buckling ultimately generates the surface rippling phenomena. This link between surface deformation and ripples also suggests a link between surface deformation and the bio-active wear debris. Other works have studied metallic films on polymer substrates, which buckle into similar patterns. These efforts suggested that thickness of the deformed layer is the dominant factor in the resulting ripple wavelength. Applying this theory to the thickness of experimentally observed surface deformation in UHMWPE correlates well with the surface rippling phenomena dimensions.
7) Tests to verify the connection between ripple wavelength and deformed layer thickness were largely inconclusive, mostly due to the inability to predict and control the thickness of the deformation layer. Computer simulations using actual wear surface geometries suggested that contact pressure and temperature would greatly affect the film thickness, but experimental results showed little change to

film thickness, suggesting that the deformation mode at the surface is not well understood.

8) The notched surface approach also revealed that larger, flake-like debris, which is consistent with adhesive wear, remains loosely attached to the polymer bulk but migrates across the surface during wear cycles. This suggests that the adhesive wear particles create a lubrication layer that is self-adhering rather than transferred to the counterface.

5.1 Challenges and Suggestions for Future Work:

Experimental efforts:

1) One potential explanation for the directionality of observed surface ripples is a directionality of stress, which is surprising considering the multi-directional quality of wear experienced. This is likely due to flexure of the sample due to friction, and could be controlled or manipulated to generate specific patterns.
2) For ease of testing procedures, the break-in period for wear was not excluded from any of the experimental testing performed in this work, which leads to a larger variation of wear debris and mechanisms observed. Future work should exclude the break-in period, if possible. Additionally, all comparison tests were performed for the same time duration, but not necessarily the same wear volume. Future work should consider using wear volume as a means to ensure that all

samples and test settings are fully beyond the break-in period and into long-term, consistent wear patterns.

3) The natural variations between samples requires a sufficient number of samples to ensure that results have the statistical power to detect differences in behavior.
4) If the surface ripples are indeed caused by the buckling of a deformed film, then the thickness of the film and its modulus should affect the ripple spacing. Measuring the modulus of the surface layer using atomic force microscopy or nano-hardness may reveal insights. Additionally, modifying the crystallinity may affect both modulus and thickness of the film. Crosslinking may also be useful to change ripple spacing.
5) Direct observation of surface deformation may be possible by using a micro-scale wear test device for use in an environmental scanning electron microscope. Initial efforts by the author showed promise, but did were not developed enough to include in this work.
6) It is still unclear whether surface ripples are a steady-state feature, or if they develop and disappear over time, or if they only appear when the contact pressure is released. Future experiments into the time-effects on ripples may prove useful in answering these questions.

Theoretical Efforts:

7) To measure wear debris complexity, rather than just using the Richardson fractal method on the particle silhouette, a technique to include *texture* of the debris should be implemented. For example, a smooth particle will have a smooth

gradient of brightness values, while a rough particle may have multiple steep jumps in brightness. Setting different threshold values will change the area of the image considered particle. Plotting these values, brightness threshold versus particle area, may reveal a fractal slope similar to the ones used in this study, which can help differentiate between wear mechanisms.

8) Previous studies in literature seem to show that crosslinking UHMWPE reduces ripple wavelength, but it is unclear why. Modulus, deformed film thickness, viscosity, yield strength, and crystalline lamella geometry were all considered, but not pursued in this work.
9) Many other suggestions besides film buckling have been put forth as the cause of ripples, some of which are listed in the introduction of the previous chapter. If alternate causes are to be considered, the author suggests starting with viscoelastic effects.
10) Importing surface geometry to computer simulations and using Von Mises yield criteria to predict material yielding did not match the experimental evidence for surface deformation. Alternate criteria for predicting deformation should be considered, including maximum shear stress, sliding between polymer chains, and the crystalline lamella effects. Molecular dynamics modeling was excluded in this study due to the technological requirements, but future efforts should include crystalline and amorphous regions.